On the Implementation of a Vegetation Baseline for ALOS/PALSAR

Paul Siqueira (UMass…), Scott Hensley, Robert Treuhaft,
Bruce Chapman, Ernesto Rodriguez *JPL*

- Open issues from May 2003
  - baseline
  - effect on crustal deformation studies
  - orbital requirements
  - temporal decorrelation
- Recommended Interferometric Observing Strategy and Resulting Benefits

One example used to find observing constraints for ALOS/PALSAR Kyoto and Carbon Cycle Initiative

System Parameter	Value
Frequency	L-Band
Wavelength	24 cm
Bandwidth	14 & 28 MHz
Noise Equivalent σ^o	$\geq$ -23 dB
Signal to Ambiguity Ratio	$\leq$ 16 dB
Thermal SNR Over Vegetation	18 dB
Platform Height	700 km
Swath Width	40 - 70 km
Resolution	7 - 44 m
Effective Number of Looks Used	64
Look Angle Range	8 - 60 degrees
Repeat Track Time	46 days

height error vs. look angle for 1km baseline

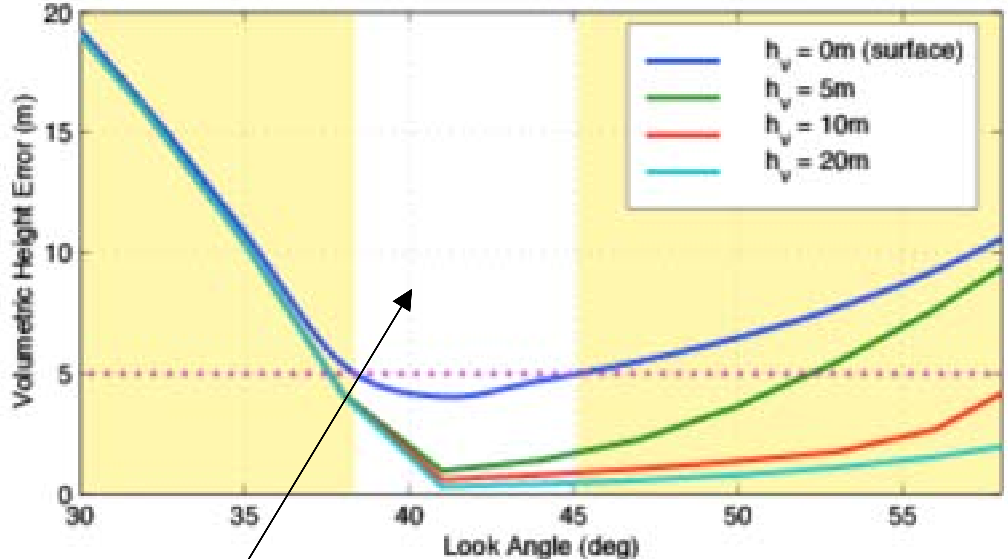

height error vs. baseline for 35 deg. look angle

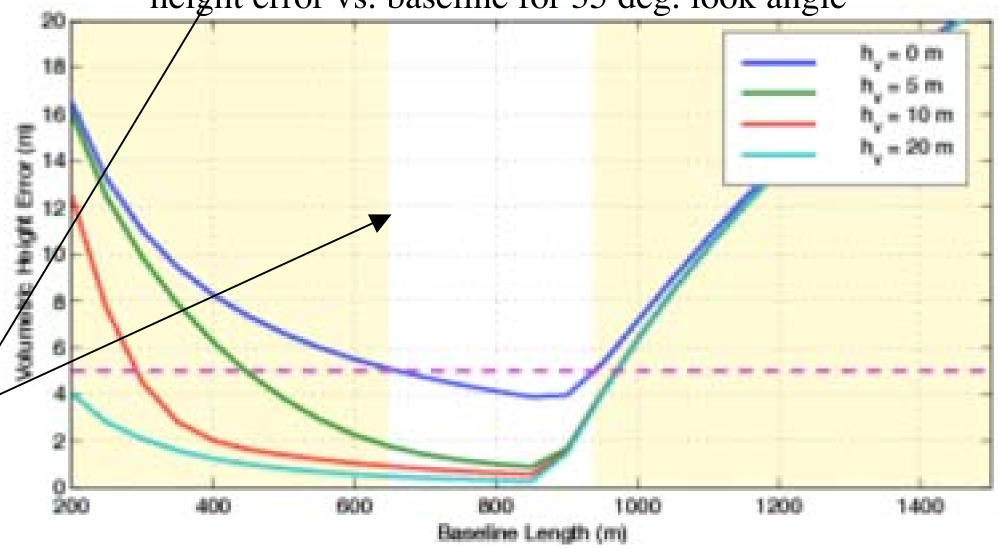

operating region

Measurement Planning: Instrument Configuration

- Often we are given access to some form or forms of measurement capability. The question we must answer as scientists is how to best utilize that resource for obtaining our objectives.

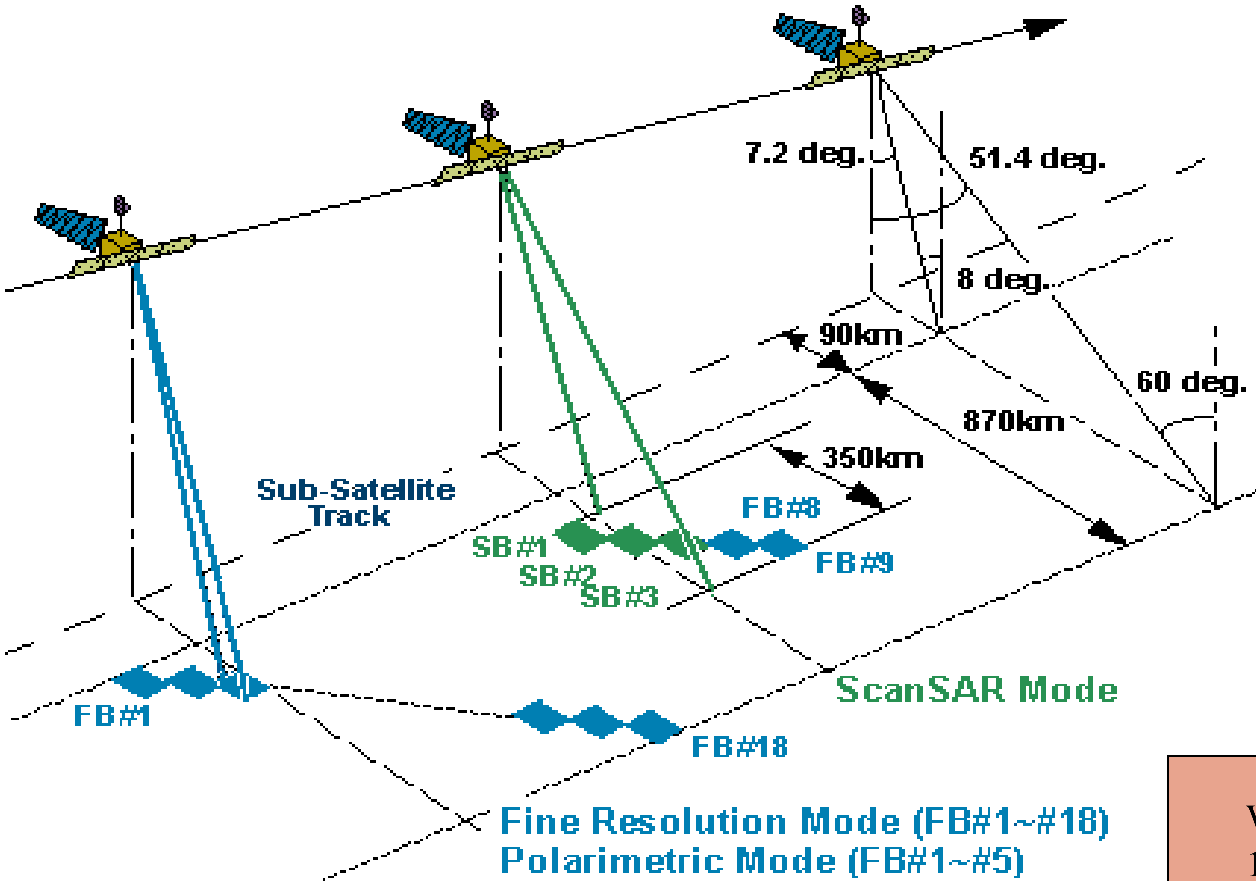

"Tree Height"
as a data product

Work Approach:
1. Methodology development
2. Regional prototype demonstration
3. Global-scale extrapolation

Interferometric Data Products

DEM from Interferometry

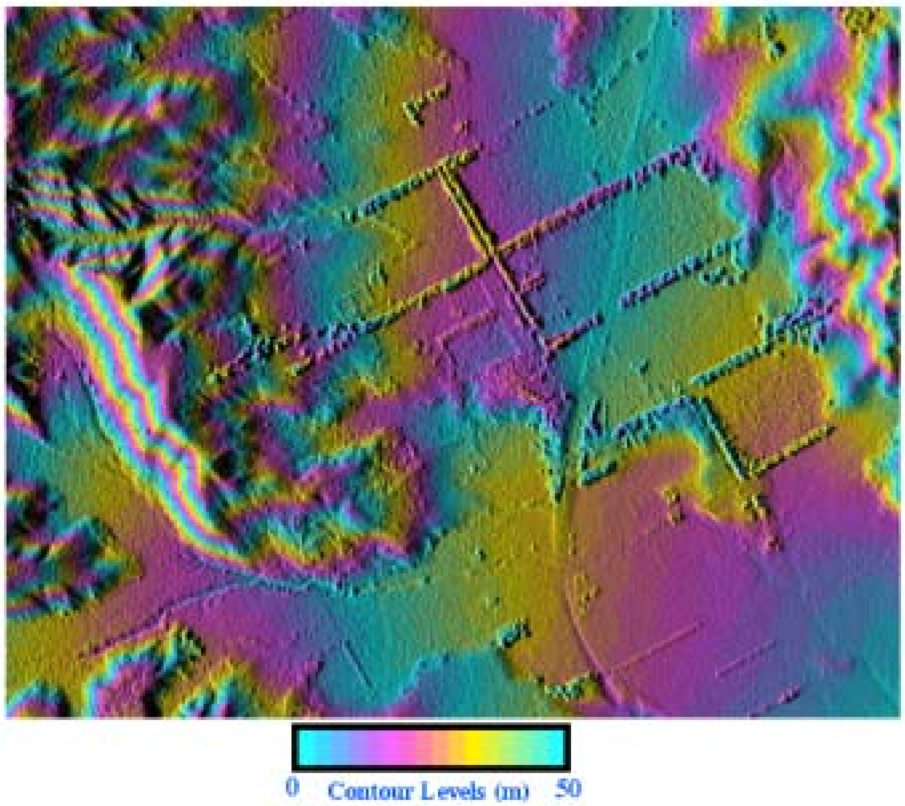

Correlation Map

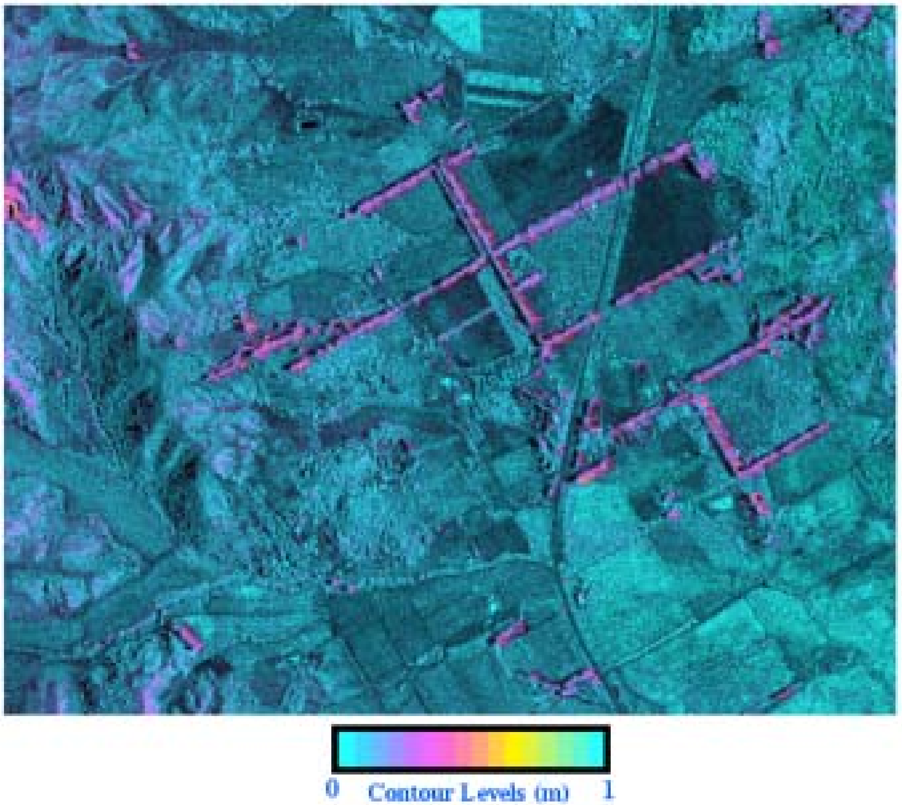

$$\gamma_{obs} = |\gamma_{obs}| e^{i\phi_{obs}} = \gamma_{vol}\gamma_{temp}\gamma_{SNR}\gamma_{geom}$$

Slicer Tree Height vs. GeoSAR Tree Heights based on X-band Correlation Magnitude

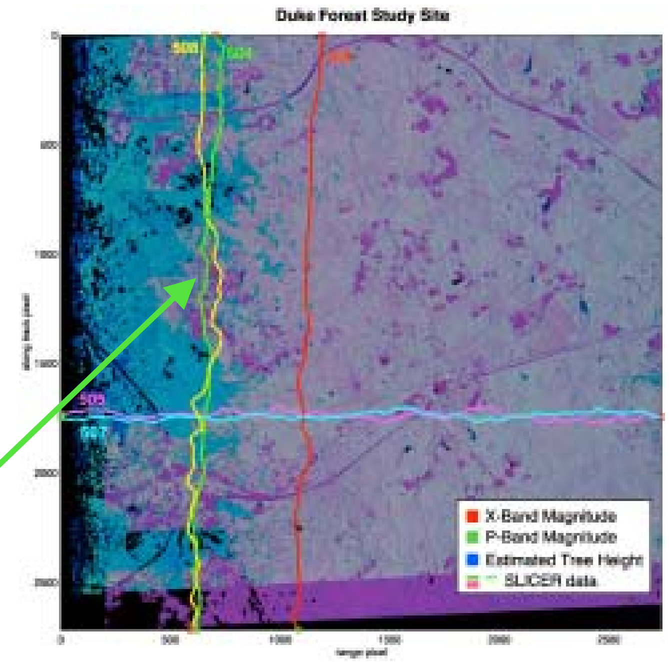

Slicer Line #504

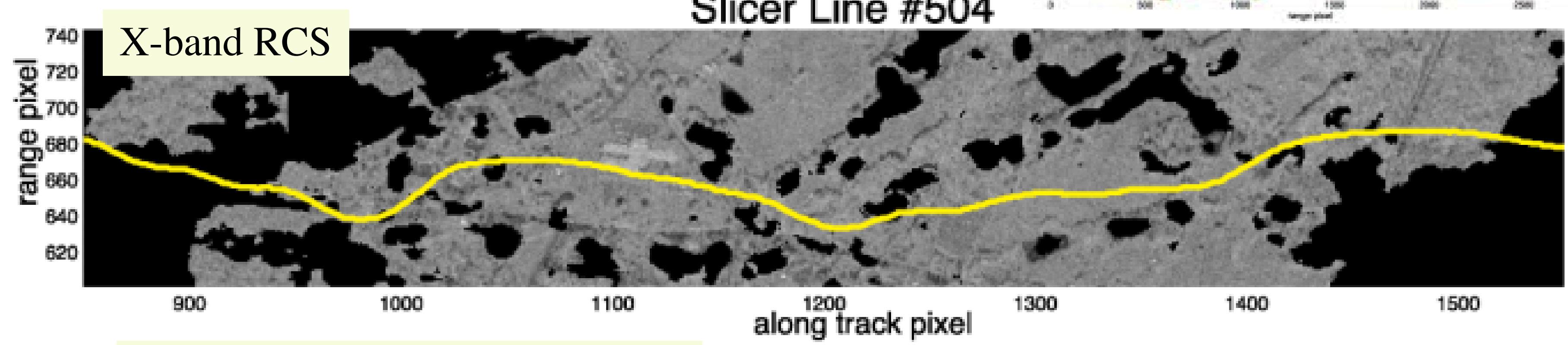

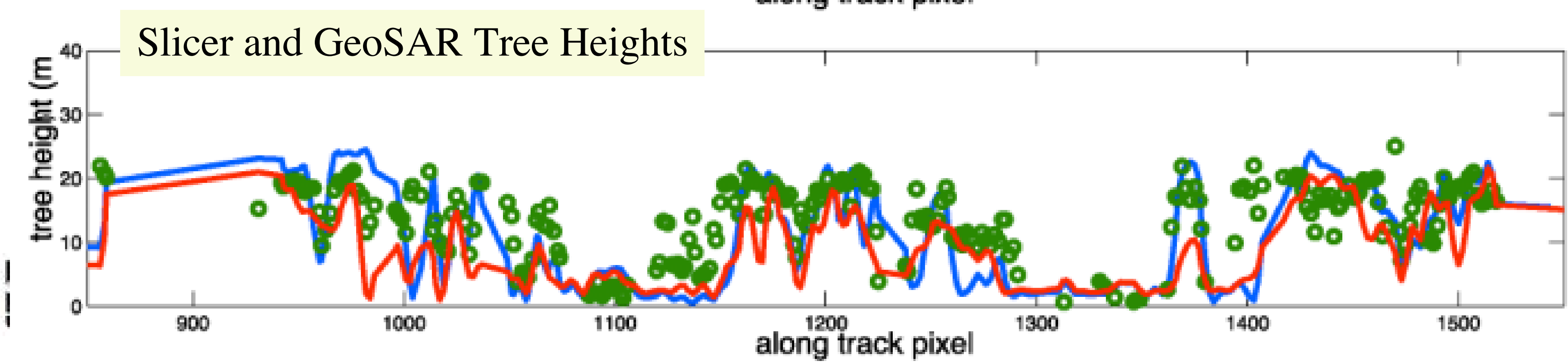

Techniques for Measuring Carbon Stored in Vegetation

Measurement Technique	Calibrated Target Measurement	Physical Interpretation	Physical Interpretation	Relation to Spatial Carbon Distribution
Lidar Profile	Lidar Height Profile	Lidar "Height", height of median energy, etc.	"Height" to Biomass conversion	Biomass to Carbon
Interferometric Correlation	Volumetric Correlation	InSAR "Height", density…	"Height" to Biomass conversion	Biomass to Carbon
Backscatter measurement	Vegetation Backscatter	Diameter at Breast Height, density, etc.	Backscatter to Biomass conversion	Biomass to Carbon
Destructive Sampling	Dry/Wet Weight	Biomass	---	Biomass to Carbon

Measurable → Modeling; Intermediate Results → Science Goal

Interferometric Correlation

• Measurement/Instrument Specifications • frequency, antenna size, baseline, resolution, etc.	• InSAR spreadsheet is well developed
• Calibration (Error Source Removal)	• developed but can be complicated
• Model for Measurement Errors	• model exists but not in spreadsheet
• Cost Model	• model exists but not in spreadsheet

Interferometric Correlation to Height Model

• Relationship between interferometric correlation and vegetation height	• model developed. currently being refined and validated
• Transformation of measurement errors into height errors	• model developed, currently being refined and validated
• Inclusion of model errors into total height errors	• imperfect model between correlation and veg. height

Height to Biomass Model

• Relationship between vegetation height and biomass	• Allometric equations exist in the forestry literature, but are not yet incorporated in this context
• Error model	• Height alone is not sufficient for biomass. Error model needs to be developed which estimates these errors.

Biomass to Carbon Model

• $C \approx 0.48(\text{Biomass})$	• believed to be well established
• Error assessment for biomass to carbon model	• believed to be well established

> 80% Done
> 60% Done
> 40% Done
> 20% Done
0% Done

Baseline Studies

B	veg. gain	deformation gain	limitations
↑	↑	↓	phase unwrapping, baseline decorr.
↓	↓	↑	SNR (thermal & ambiguities)

Tree Height Estimation from Radar Interferometry

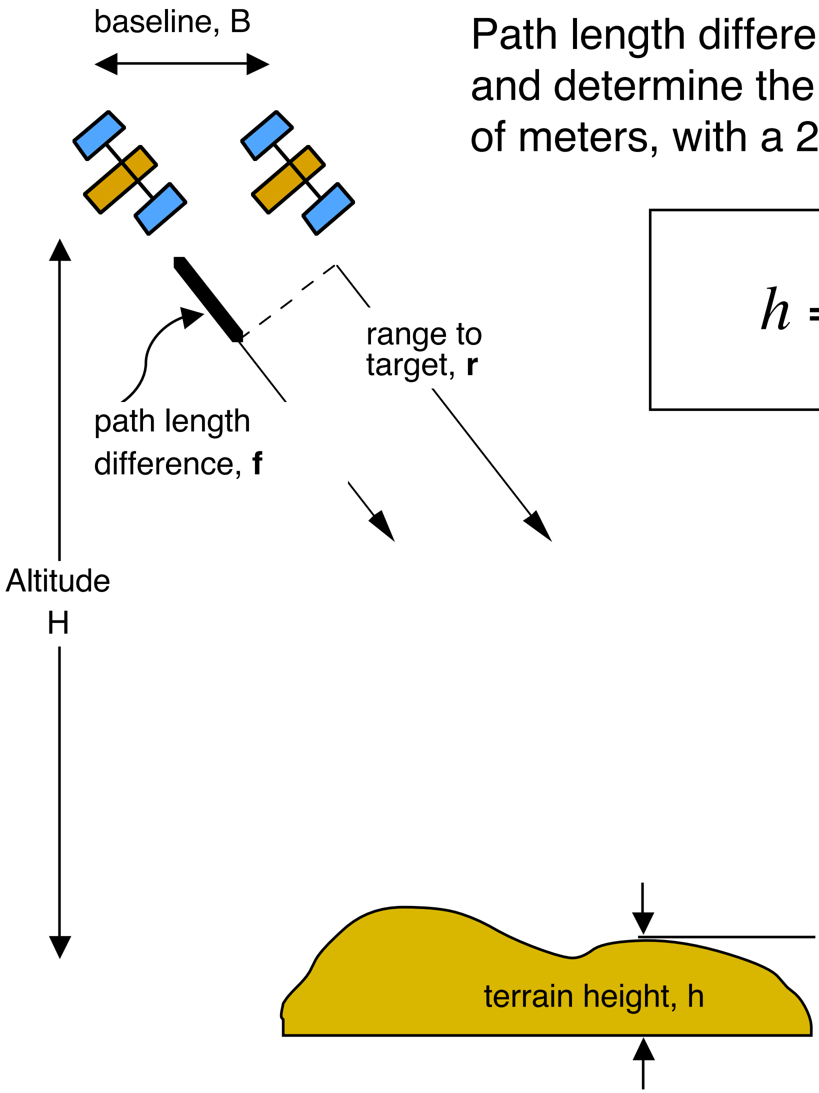

Path length difference can be used to resolve positional ambiguity and determine the height of the terrain. Accuracy is on the order of meters, with a 25m resolution

$$h = H - \rho \cos\left(\sin^{-1}\left(\frac{\lambda\phi}{4\pi B}\right)\right)$$

When the signal return comes from multiple heights, a unique signature is observed by the interferometer

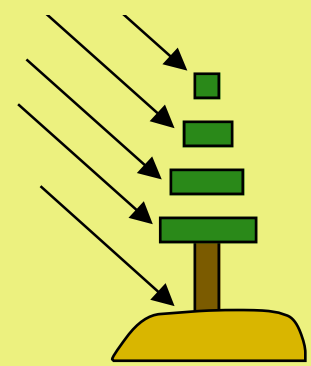

Interferometric Modeling

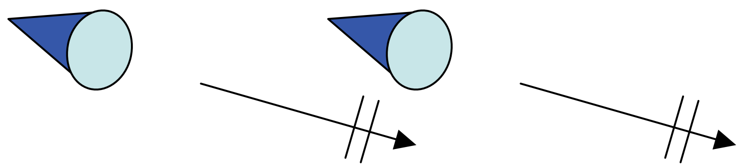

Single Antenna Backscatter

$$\left\langle |E_1|^2 \right\rangle = A^4 \int_{vol} W_r^{\,2} W_\eta^{\,2} e^{-\kappa z/\cos\theta} \rho(z) \left\langle f_b^{\,2} \right\rangle d^3 r$$

Two Antenna Interferometry

$$\gamma = \left\langle E_1 E_2^{*} \right\rangle = A^4 \int_{vol} e^{-ik_z z} W_r^{\,2} W_\eta^{\,2} e^{-\kappa z/\cos\theta} \left\langle f_b^{\,2} \right\rangle d^3 r$$

height dependent
phase term

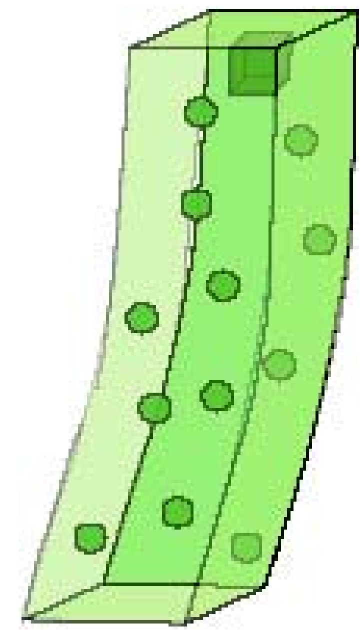

Approach to System/Measurement Design

- Explore the effects of changing baseline, B, and look angle, θ, on the estimate error.

$$h_{v,est} \propto \gamma_{vol} \propto \gamma_{meas} \propto f\,(\text{instrument config;forest params})$$

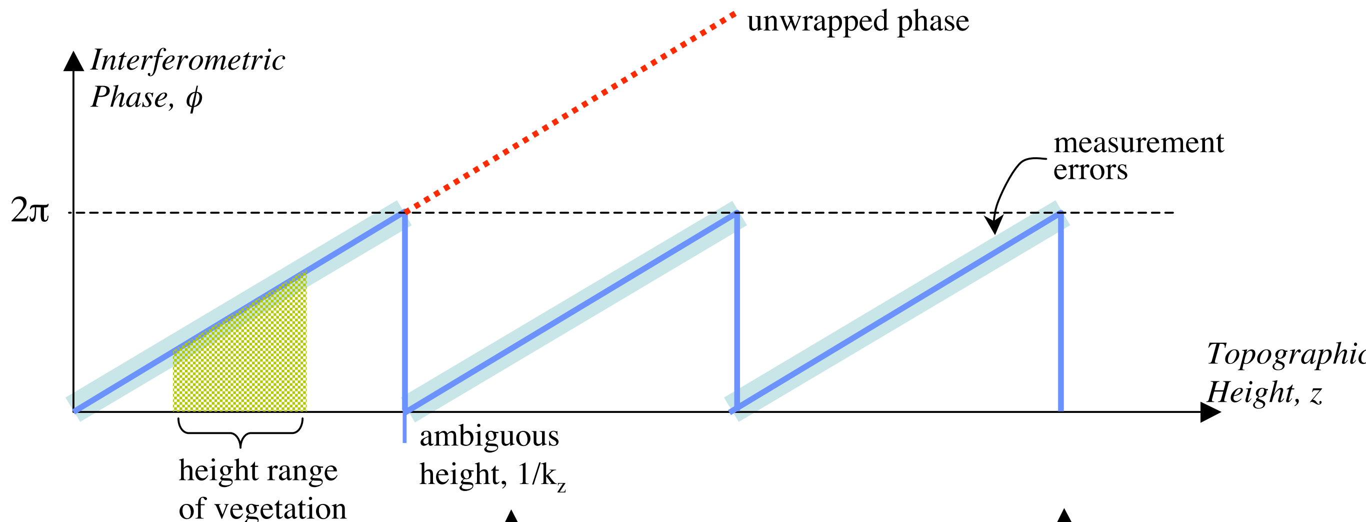

slope of line is set by the sensitivity of interferometric phase to height

$$k_z = \frac{akB\cos(\theta - \alpha)}{R\sin\theta}$$

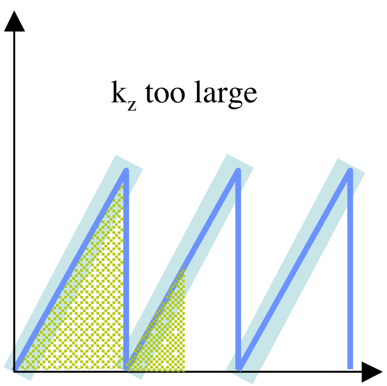

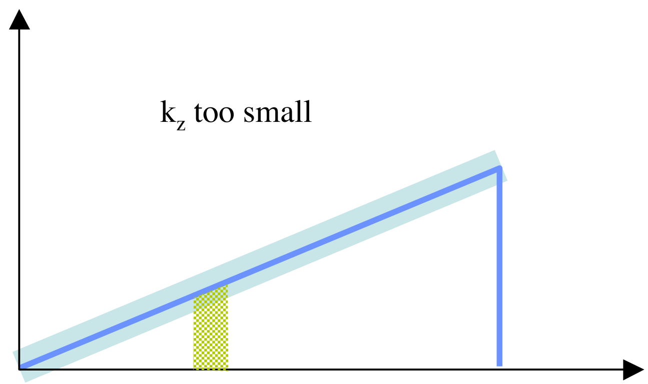

Contributions to the observed correlation signature

- Geometric Decorrelation

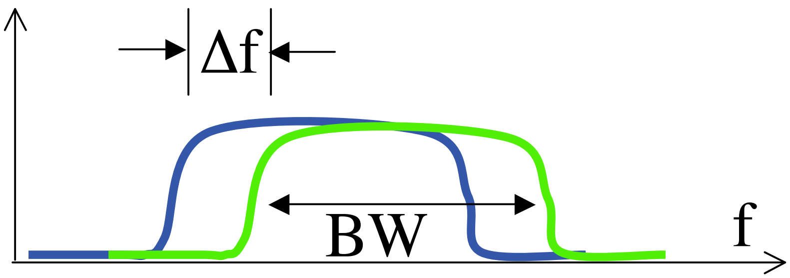

$$\Delta f = \frac{c\,B\cos(\theta-\alpha)}{2\ \ r_0\ \lambda\tan(\theta-\tau_y)}$$

$$\gamma_{geom} \approx 1 - \frac{c\,B\cos(\theta-\alpha)}{2\ BW\, r_0\ \lambda\tan(\theta-\tau_y)}$$

- Thermal Noise

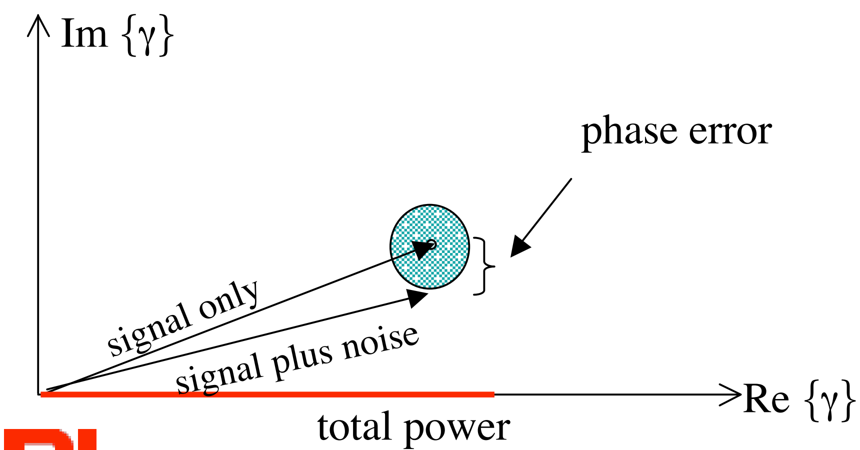

$$\gamma_{SNR} = \frac{S}{S(1+\alpha)+N_{th}}$$

Choose kz to maximize signal and minimize errors

max baseline for 28 MHz BW L-band signal (ALOS/PALSAR) set by upper limit to decorrelation

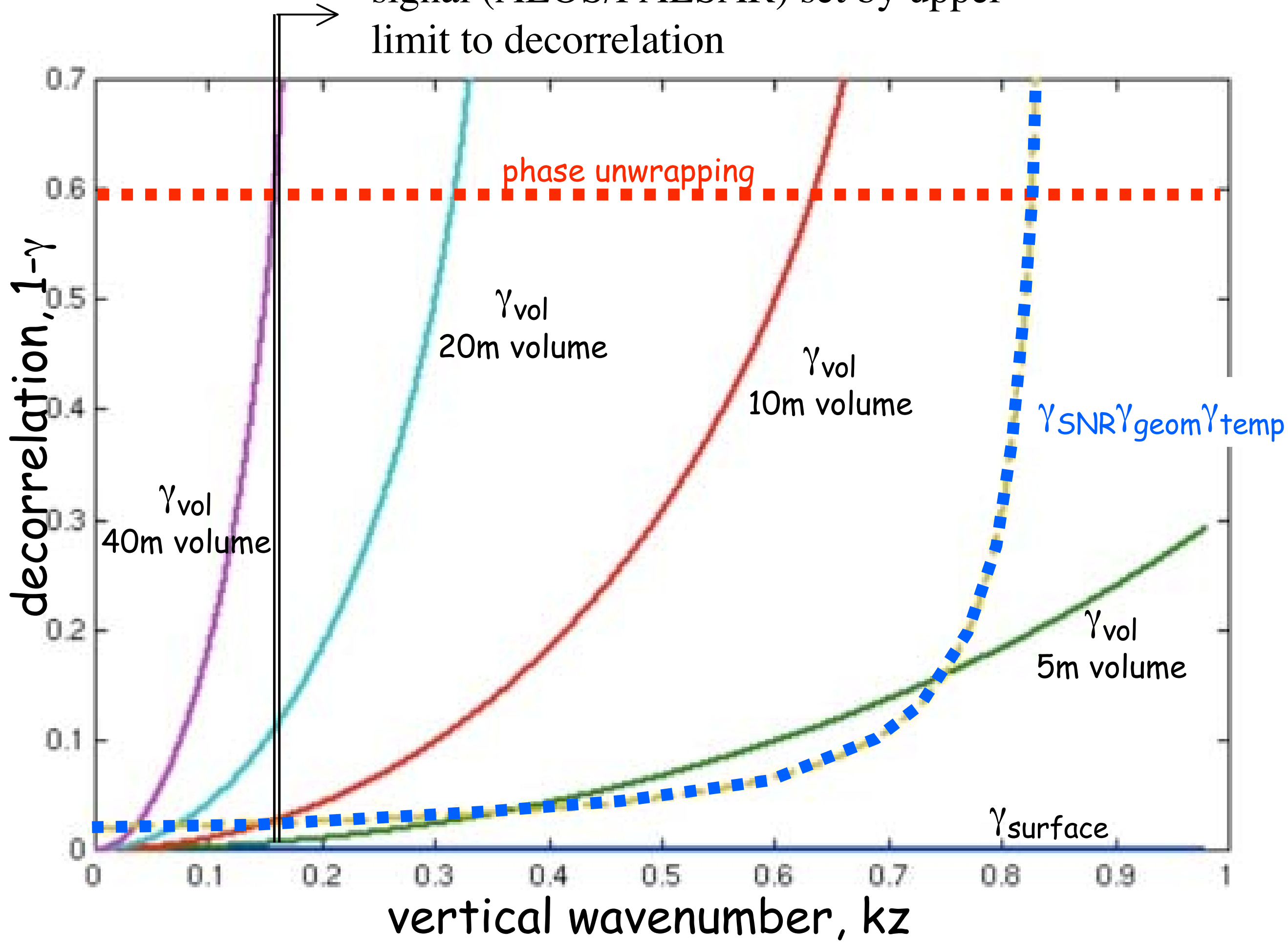

small baseline ----> large baseline

- large baseline desired to maximize sensitivity to volumetric decorrelation

  (short volumes have small decorrelation signatures)
- maximum baseline is limited by
  - loss of signal due to the wavenumber shift (Prati filtering)
  - maximum decorrelation allowable for phase unwrapping (γ=0.4)
- simple volumetric model used to demonstrate this tradoff in figure at left.
- minimum detectable height set by observational errors

Some Comparisons

- Observational characteristics for various interferometers can be compared with a proposed InSAR observation that would be sensitive to vegetation

Sensor	Altitude (km)	θ, α (deg)	B, λ (m)	k_z (rad/m)	h_{ambig} (m)	BW, B_{crit} (MHz, m)
GeoSAR X	10,000	45, 0	2(2.6), 0.03	0.08	160	160, 230
GeoSAR P	10,000	45, 0	2(20), 0.87	0.02	310	160, 6500
AIRSAR C	10,000	45, 65	2(2.5), 0.056	0.05	120	40, 85
SRTM	230,000	40, 45	60, 0.056	0.03	240	10, 600
DLR - L	3,000	39, 0	2(15), 0.24	0.24	27	100, 260
ALOS/PALSAR	700,000	35, 0	2(800), 0.24	0.07	90	28, 13400

Repeat Pass Cross-Track Baseline

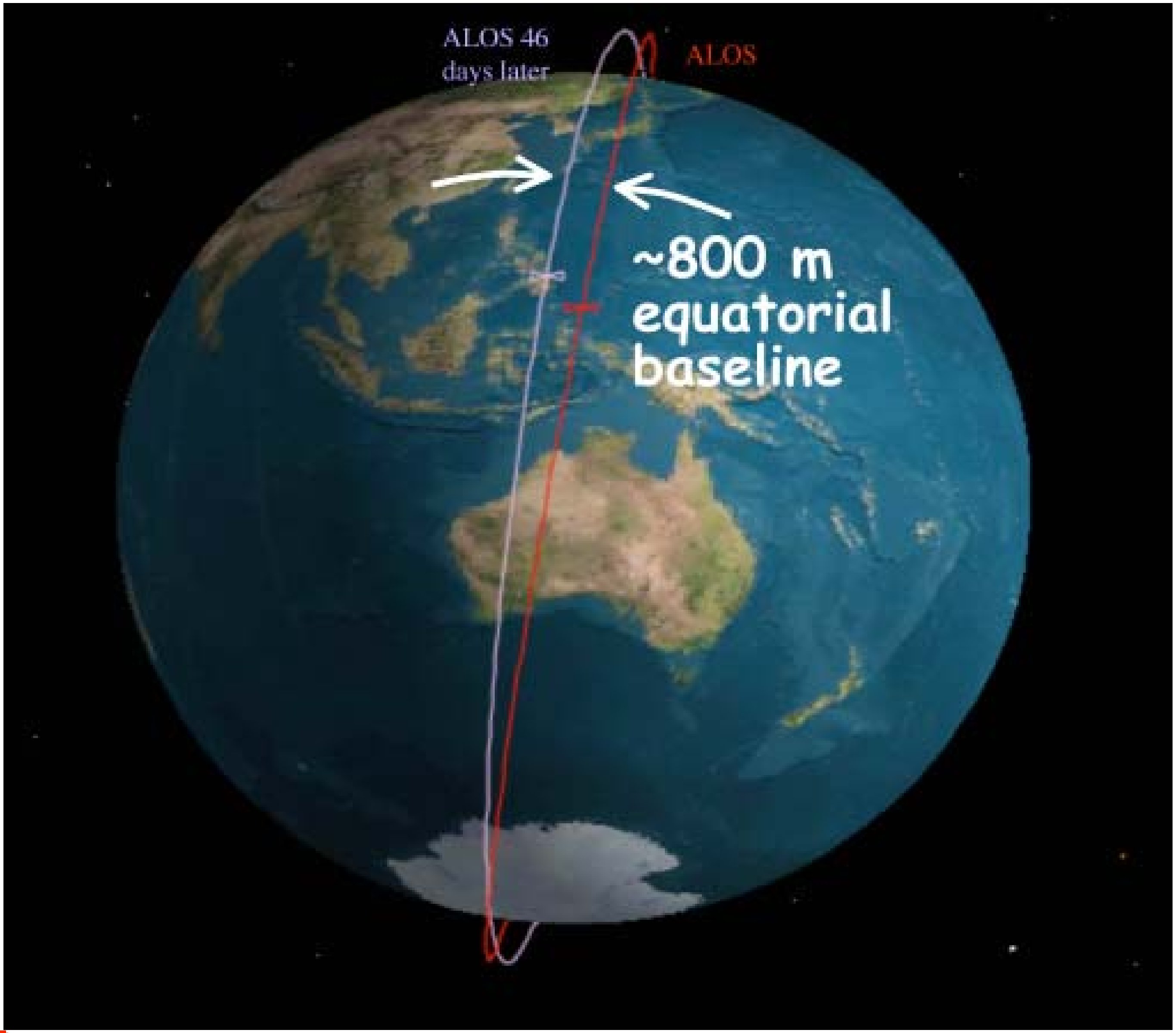

Implementation Issues

• Baseline changes as a function of latitude

• Very small amount of lateral thrust (<0.001 m/s) applied to spacecraft at equator crossing to achieve "time of day" shift in crossing. Typical thrust budget is ≈ 100 m/s.

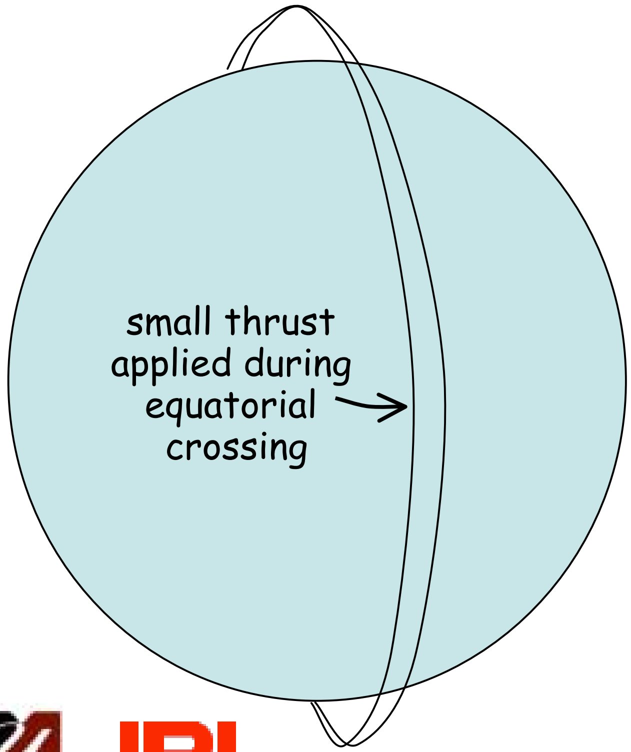

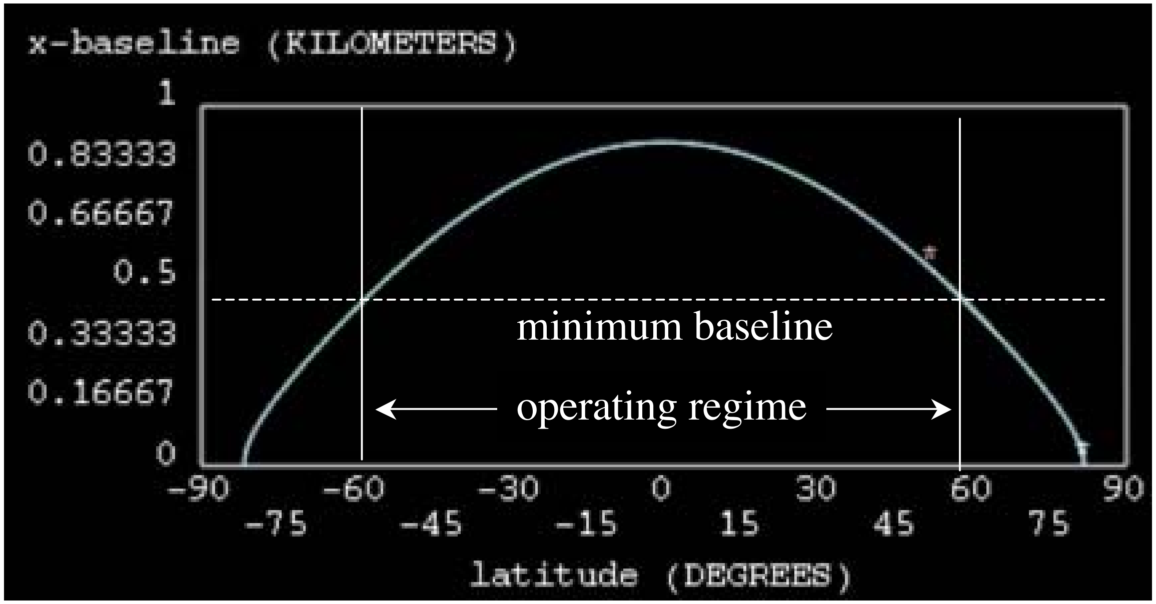

Drag-free Ground Track Walk at the Equator

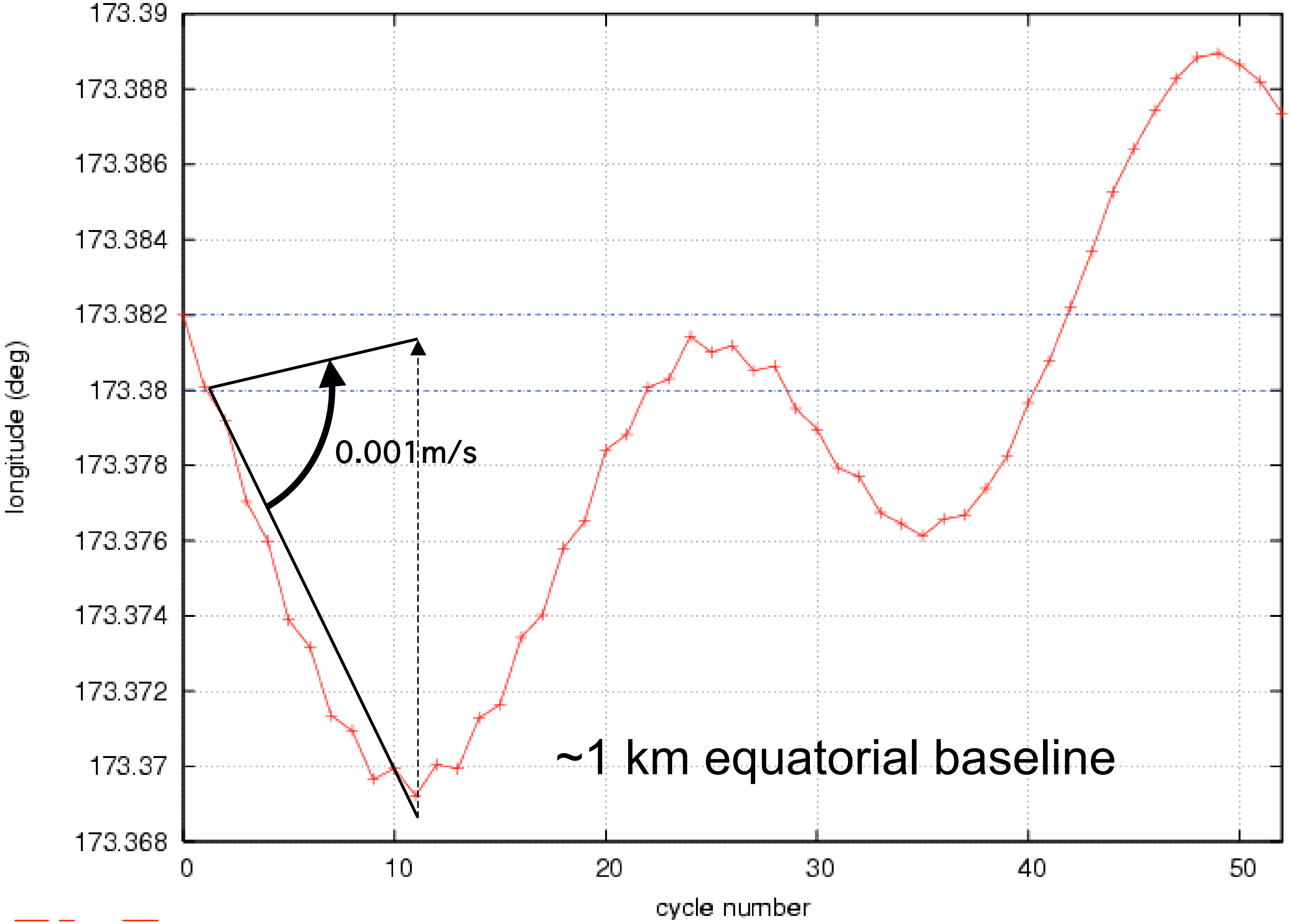

Deformation

InSAR

Potential Partners

Interferometric Synthetic Aperture Radar

Mission Objective: *The InSAR mission objective is to provide the first dedicated spaceborne interferometry mission to precisely map Earth surface deformation due to tectonic, volcanic, and glacial processes. The resulting data will uniquely allow characterization and quantification of underlying processes enabling predictive models.*

Preliminary InSAR Fundamental Science Targets

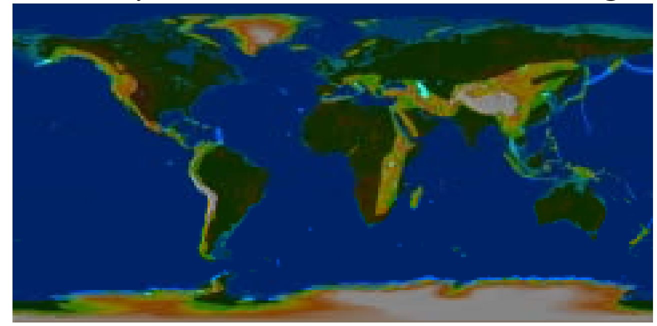

Science Objectives:

- *Characterize and understand strain changes in tectonically active areas leading to and following major earthquakes*
- *Characterize three dimensional magma movements leading to better prediction of volcanic eruptions*
- *Assess the impact of ice sheet and glacier system dynamics on sea level rise and characterize temporal variability*

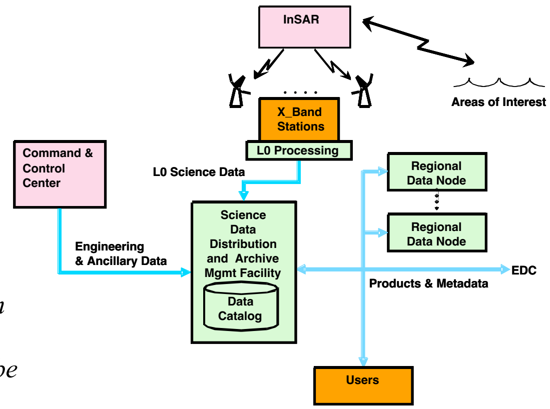

Operations:

- *Simple 8-day repetitive mission cycle*
- *Two S/X-band Ground Stations*
  ASF and Svalbard
- *Selected ground automation*
- *Distributed processing architecture*

Mission Requirements:

- *5-year lifetime*
- *10-minutes of data per orbit (average)*

Navigation and Orbit:

- *Sun synchronous 6am/6pm*
- *760 km, 98.5°*
- *250 m diameter orbital tube*

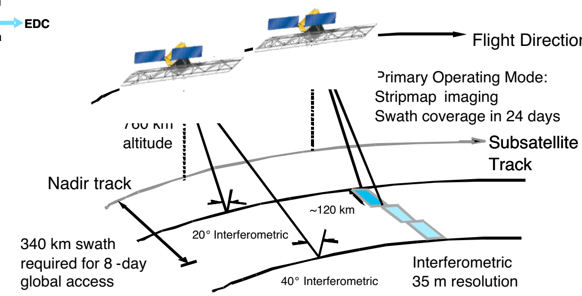

Project Implementation:

- *JPL instrument electronics build*
- *Commercial spacecraft bus; antenna panels, structure, and deployment mechanism*
- *Precision GPS as GFE to spacecraft bus contractor*
- *JPL I&T of phased-array antenna and radar electronics*

Measurement Technology:

- *Repeat pass radar interferometry*
- *3-D vector deformation by observing*
  - *while pointing to the left and right*
  - *on ascending and descending orbits*

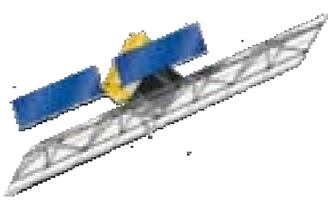

Flight System:

- *Enhanced RSDO Catalog bus*
- *GPS for Precision Orbit Determination/Nav.*
- *Selected-to-full redundancy*
- *Mass* *1350 kg wet (CBE + cont.)*
- *Downlink* *300 Mbps X-band*
- *Storage* *256 Gb minimum*
- *Maneuvers* *0.1°/sec left/right pointing*
- *Pointing* *0.04° 3-sigma yaw/pitch*
  0.25° 3-sigma roll

Launch System:

- *Delta II 2920-10*
- *3150 kg to 760 km*
- *57% Launch Margin*
- *April 2009, VAFB*

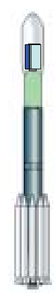

Payload System:

- *L-band single-polarization (HH) radar*
- *Split spectrum for ionospheric correction*
- *Full redundancy of radar electronics*
- *Stripmap, High-Resolution and ScanSAR Modes*
  - *Primary operating mode – Stripmap Mode*
    (continuous strip-mapping with 3 possible beams)
- *13.8 m x 2.5 m antenna aperture*
- *Deployable antenna structure*
- *Mass* *600 kg (CBE +30%)*
- *Power* *1800 W peak (CBE +30%)*
- *Data rate* *130 Mbps average (CBE)*

Observing Sensitivity to Deformation

- Observed interferometric phase is sensitive to the surface deformation projected onto the look direction.

$$D_{\|} \equiv \hat{l}_1 \cdot \overline{D} = \phi \frac{\lambda}{4\pi} + B \sin(\theta - \alpha)$$

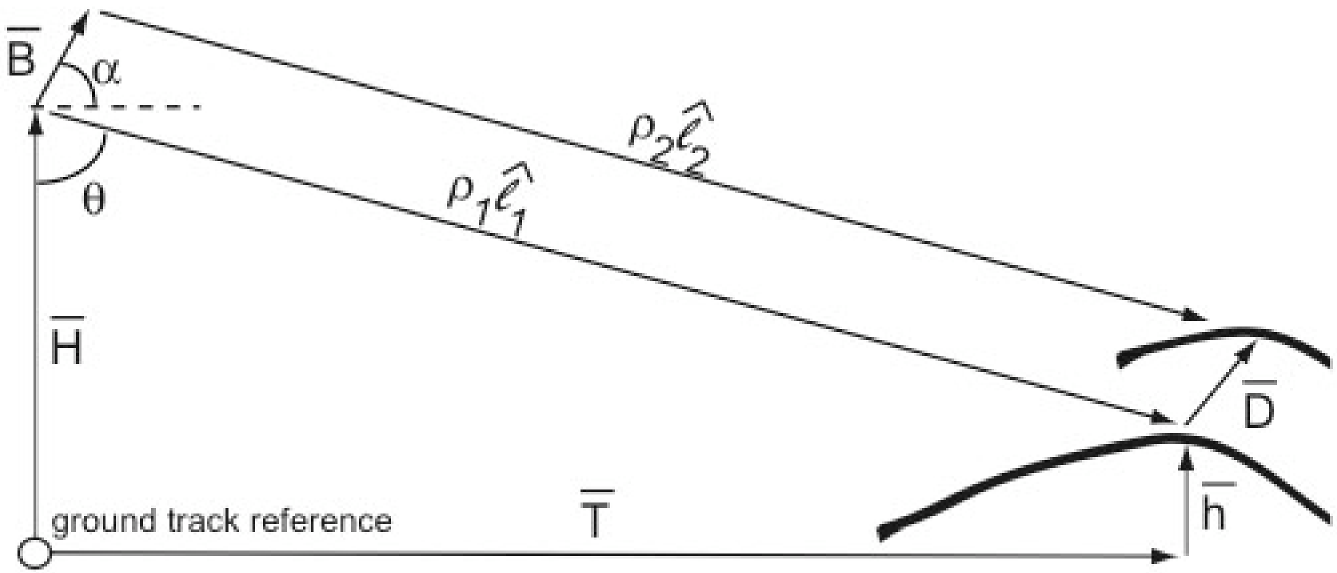

$$\rho_1 = \overline{T} \cdot \hat{l}_1 + \overline{h} \cdot \hat{l}_1 - \overline{H} \cdot \hat{l}_1$$

$$C_N = \frac{\langle E_1 E_2^* \rangle}{\sqrt{\langle |E_1|^2 \rangle \langle |E_2|^2 \rangle}} = \gamma e^{j\phi}$$

$$\rho_2 = \overline{T} \cdot \hat{l}_2 + \overline{h} \cdot \hat{l}_2 + \overline{D} \cdot \hat{l}_2 - \overline{H} \cdot \hat{l}_1 - \overline{B} \cdot \hat{l}_2$$

$$\phi = 2k(\rho_2 - \rho_1) \approx 2k\hat{l}_1 \cdot (\overline{D} - \overline{B})$$

Error Budget

- The instrument measurement requirements are split the error into its constituent sources.

$$\sigma^2_{D_{\|}} - \left(\frac{\partial D_{\|}}{\partial \phi}\right)^2 \sigma^2_{\phi} + \left(\frac{\partial D_{\|}}{\partial \lambda}\right)^2 \sigma^2_{\lambda} + \left(\frac{\partial D_{\|}}{\partial B}\right)^2 \sigma^2_{B} + \left(\frac{\partial D_{\|}}{\partial \theta}\right)^2 \sigma^2_{\theta} + \left(\frac{\partial D_{\|}}{\partial \alpha}\right)^2 \sigma^2_{\alpha}$$

$$\sigma^2_{D_{\|}} = \left(\frac{\lambda}{4\pi}\right)^2 \sigma^2_{\phi} + \left(\frac{B}{\lambda}\sin\left(\theta-\alpha\right)\right)^2 \sigma^2_{\lambda} + \sigma^2_{B} + \left(\frac{B\cos\left(\theta-\alpha\right)}{\rho\sin\theta}\right)^2 \left[\sigma^2_{h} + \sigma^2_{H} + \cos^2\theta\,\sigma^2_{\rho}\right]$$

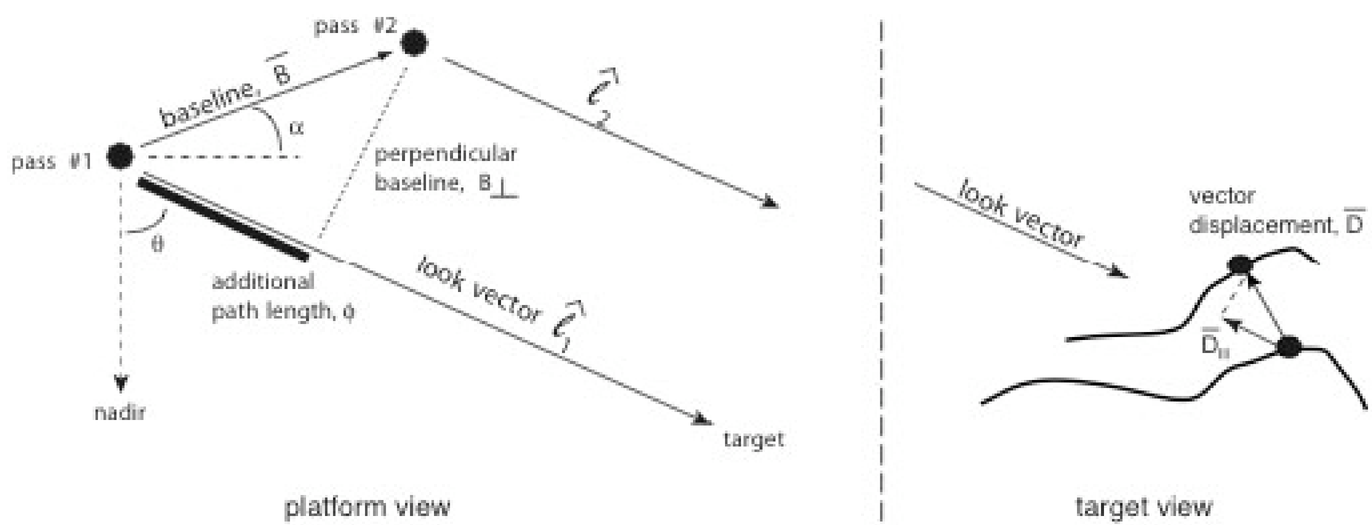

UMASS JPL

Topographic Leakage

- Uncertainty in topography will induce a signature proportional to the error in topographic knowledge.

$$D_{\parallel} \equiv \hat{l}_1 \cdot \overline{D} = \phi \frac{\lambda}{4\pi} + B \sin(\theta - \alpha)$$

$$\sigma_{D_{\parallel}}^2 = \left(\frac{\lambda}{4\pi}\right)^2 \sigma_\phi^2 + \left(\frac{B}{\lambda}\sin(\theta-\alpha)\right)^2 \sigma_\lambda^2 + \sigma_B^2 + \left(\frac{B\cos(\theta-\alpha)}{\rho\sin\theta}\right)^2 \left[\sigma_h^2 + \sigma_H^2 + \cos^2\theta\,\sigma_\rho^2\right]$$

- Three-pass differential interferometry can be used to reduce this effect, by essentially estimating the topography and removing it.
- Phase noise is still an issue

$$\sigma_h^2 = \sigma_\phi^2 / k_z^2$$

$$\sigma_{D_{\parallel}}^2 \approx \left(\frac{\lambda}{4\pi}\right)^2 \left(1 + \frac{B_{\parallel}^2}{B_z^2\left(1-\delta_{geom}\right)^2}\right)\sigma_\phi^2 + \left(\frac{B}{\lambda}\sin(\theta-\alpha)\right)^2 \sigma_\lambda^2 + \sigma_B^2$$

Single-side Orbit Tube Geometry

- Orbital tube is defined in the perpendicular look direction by geometric decorrelation, the fringe rate and topographic errors

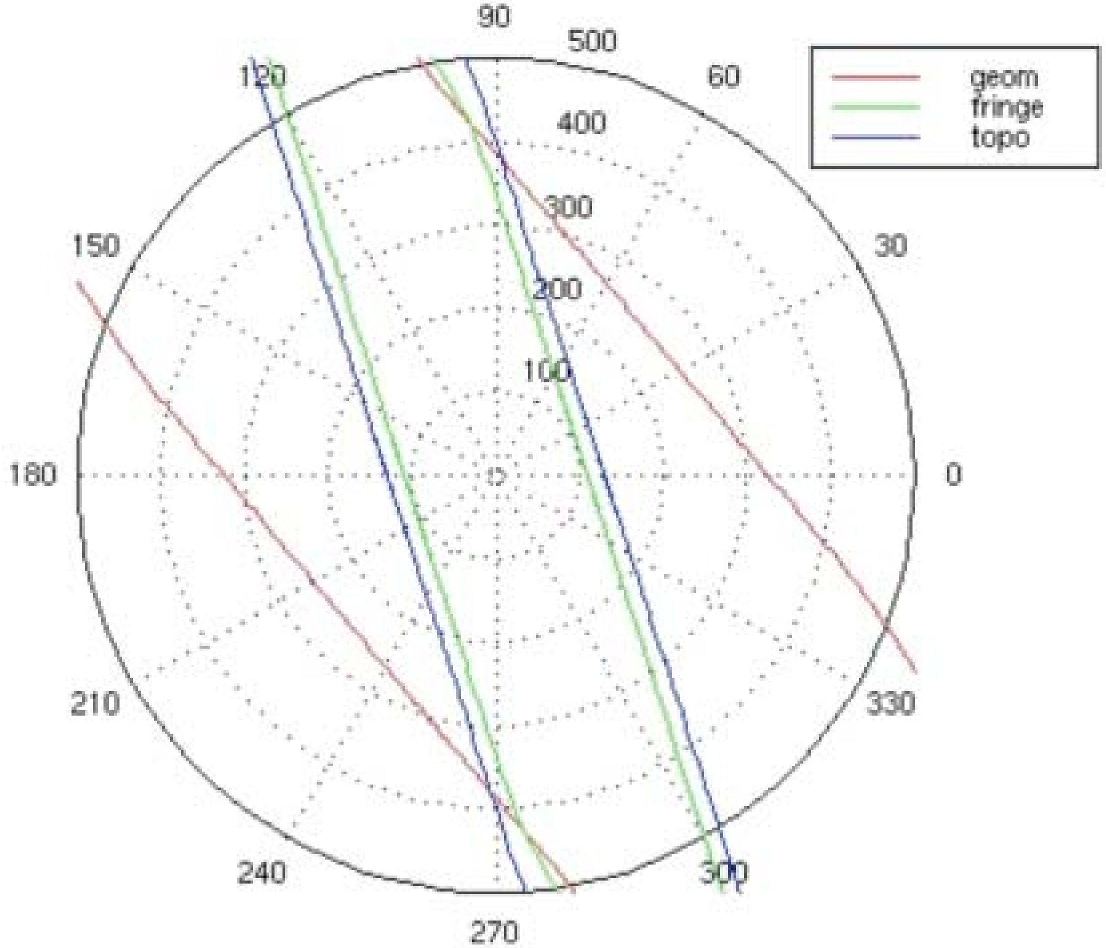

Two-Side Orbital Tube Geometry

- Orbital tube geometry and dimension is set by knowledge of the look angle (i.e. topography) and baseline decorrelation.
- Shown below is the error induced in the deformation measurement due to a 10m accuracy in the surface topograpy.

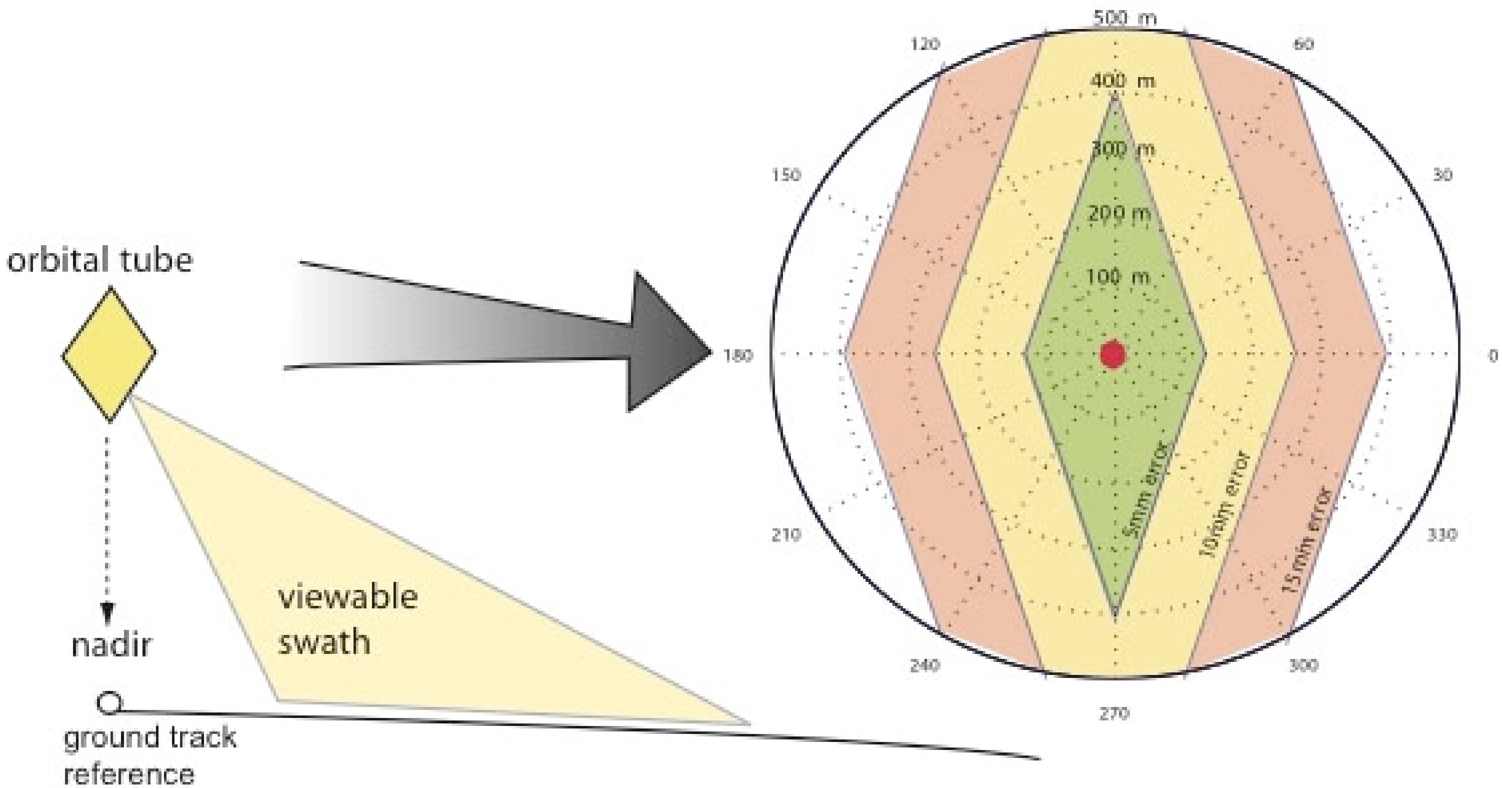

$$D_{\|} \equiv \hat{l}_1 \cdot \overline{D} = \phi \frac{\lambda}{4\pi} + B \sin(\theta - \alpha)$$

Temporal Decorrelation

Temporal Decorrelation

- Need for a well calibrated signal
  - understand error sources
  - provide ability to unwrap desired signature from other observational artifacts.
- Devise an efficient observing strategy
- Assess possibility of removing this effect

- Observed correlation is modeled as the combination of a variety of sources

$$\gamma_{obs} = \gamma_{vol}\gamma_{SNR}\gamma_{geom}\gamma_{temp}$$

$$\Rightarrow \quad \gamma_{vol} = \frac{\gamma_{obs}}{\gamma_{SNR}\gamma_{geom}\gamma_{temp}} = f(h_v)$$

$$h_v = f^{-1}(\gamma_{vol})$$

Estimation of γ_{temp}

- Model can be inverted to solve for the temporal decorrelation

$$\gamma_{temp} = \frac{\gamma_{obs}}{\gamma_{vol}\gamma_{SNR}\gamma_{geom}}$$

- Would like to include target type as well as SNR and geometric decorrelation parameters into estimate

$$\gamma_{vol} \le \mathrm{sinc}\left(k_z h_v / 2\right) \qquad \gamma_{geom} \approx 1 - \frac{2B\cos(\theta - \alpha)\Delta\rho}{\lambda\rho\tan(\theta - \tau_y)}$$

$$\gamma_{SNR} = \frac{S}{S(1+\alpha) + N_{th}}$$

$$\Rightarrow \left(1 - \gamma_{temp}\right) \le 1 - \frac{\gamma_{obs}}{\gamma_{vol}\gamma_{SNR}\gamma_{geom}}$$

Duke Forest, North Carolina
(Oct 9 & 10, 1995; kz = 0.01 rad/m)

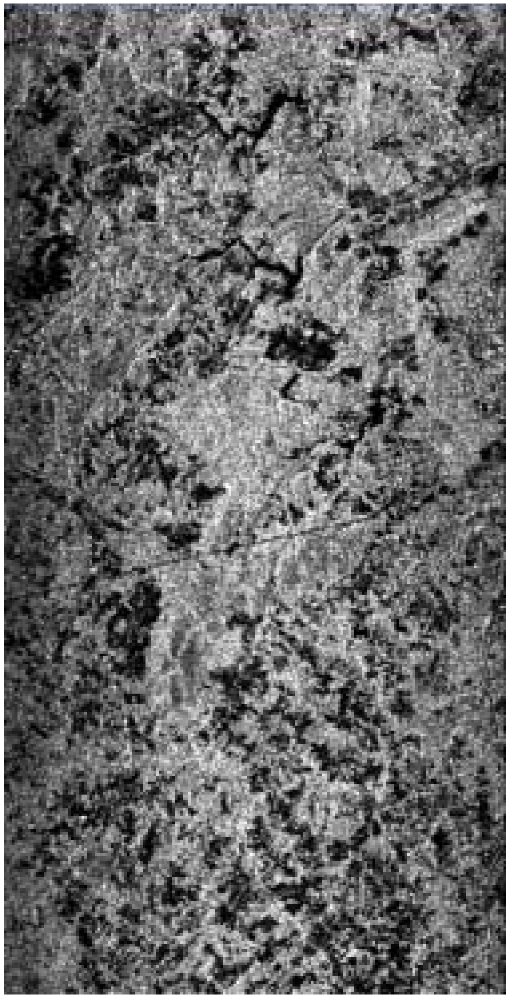

backscatter

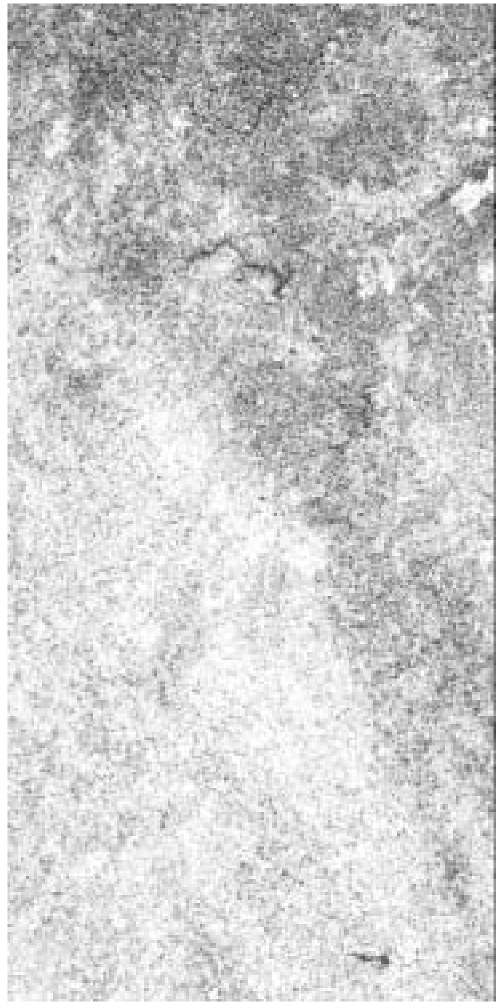

correlation

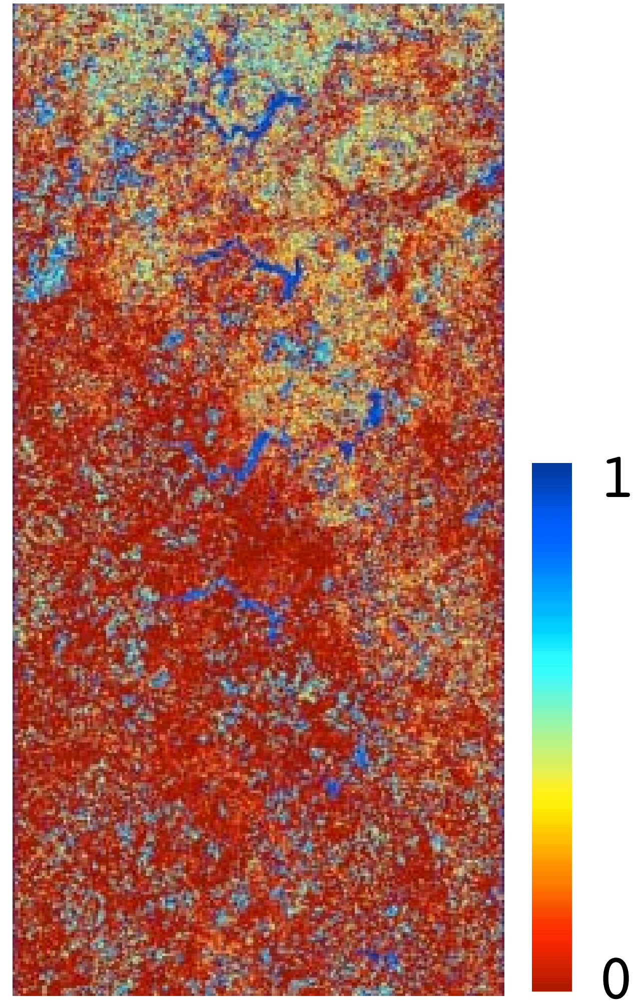

temporal decorrelation

Raco, Michigan
(Oct 8 & 9, 1994; kz = 0.04 rad/m)

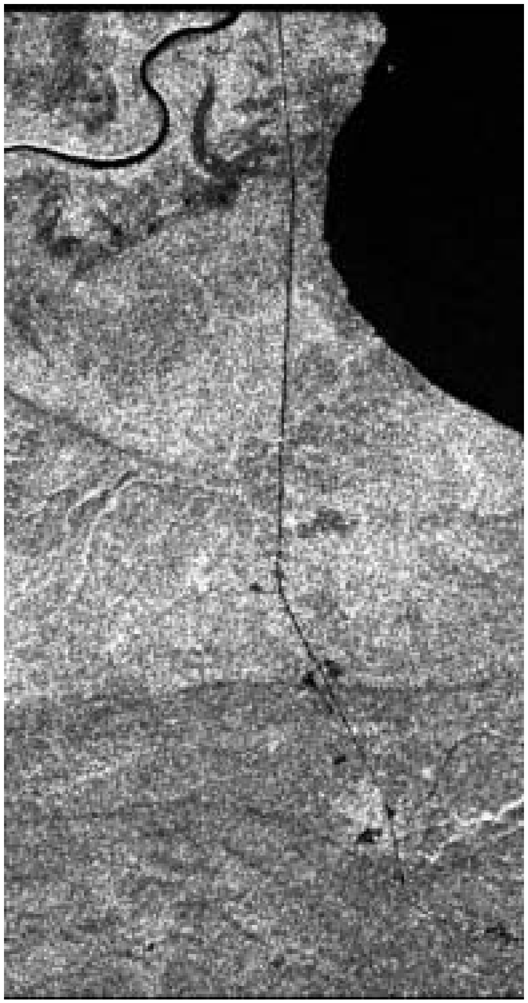

backscatter

correlation

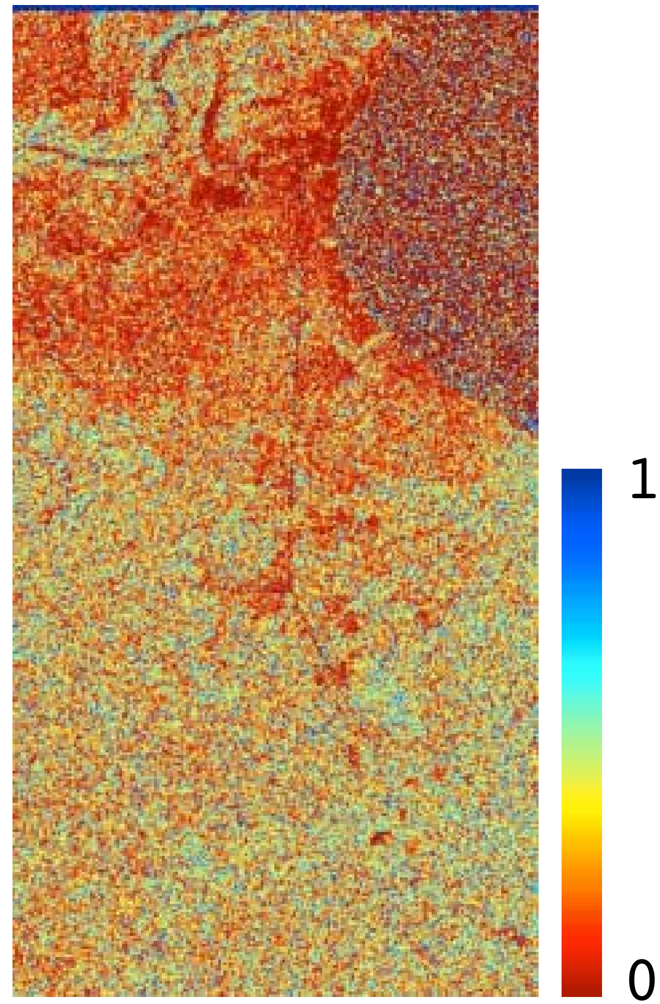

temporal decorrelation

Raco, Michigan

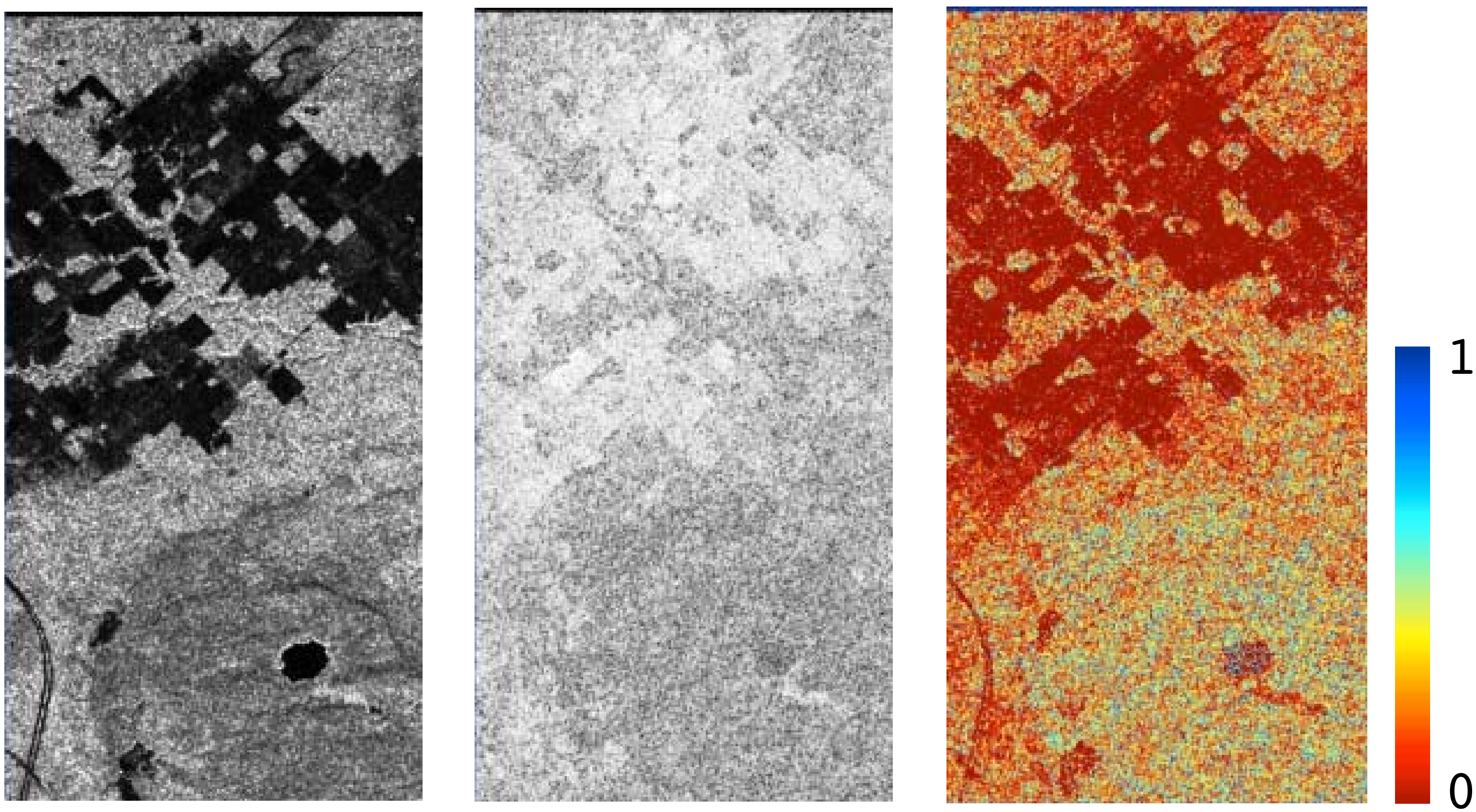

backscatter | correlation | temporal decorrelation

Estimates of Temporal Decorrelation over Raco

- Both surfaces and vegetated regions show evidence of significant temporal decorrelation even after assuming 30m tall vegetation.
- Surfaces show less decorrelation, as would be expected

$$1-\gamma_{temp} \leq 1-\frac{\gamma_{obs}}{\gamma_{vol}\gamma_{SNR}\gamma_{geom}}$$

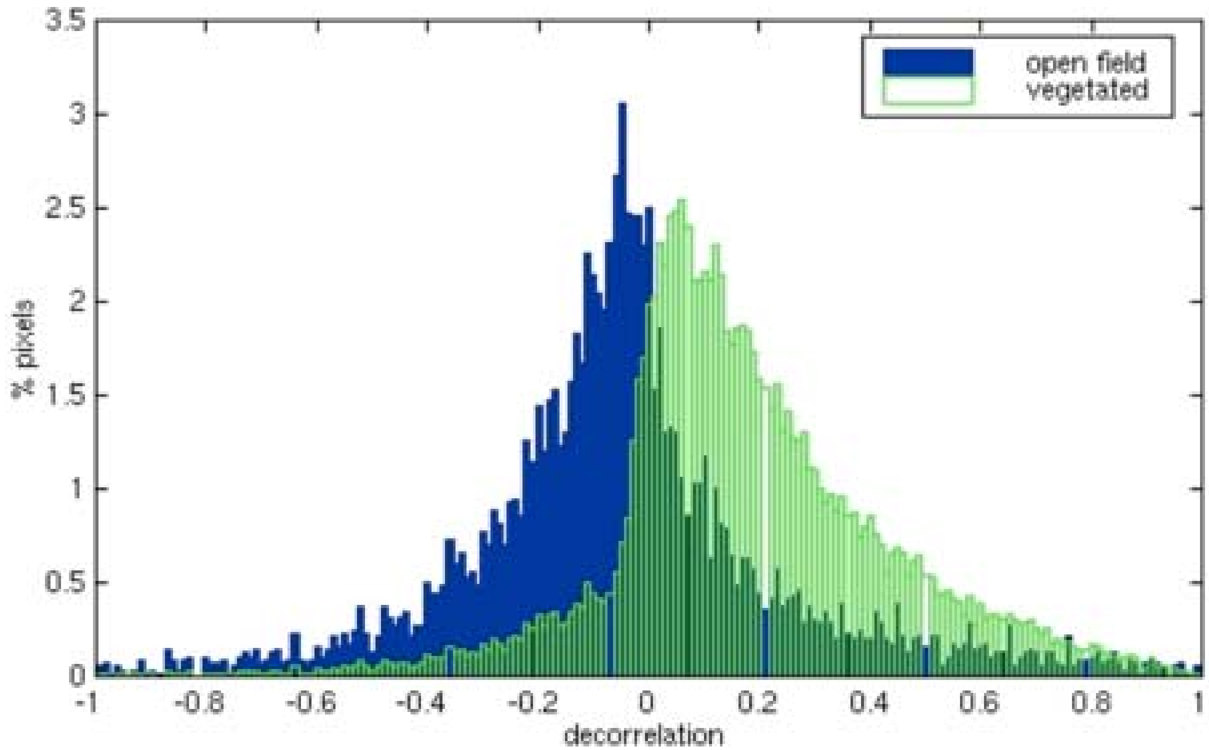

Source of Temporal Decorrelation ?

Raco, MI Early October, 1994

Estimation of γ_{temp}

- Note that γ_{temp} will have a statistical distribution based on our ability to estimate contributing sources.

$$\gamma_{temp} = \frac{\gamma_{obs}}{\gamma_{vol}\gamma_{SNR}\gamma_{geom}}$$

- Ultimately, resolution can be traded off to increase estimate accuracy

- At what Δt does temporal decorrelation become an issue?
  - one minute?
  - one hour?
  - one day?
  - one week?
  - one month?

- Need to investigate more closely the time dependence of temporal decorrelation …

La Selva &
AIRSAR

Experiment Location

uelle
Pital
Chilamate
PUERTO VIEJO
Estaci—n Biol—gica La Selva
El Tigre
La Palmera
La Virgen
Aguas Zarcas
Venecia
Semillero
Cariari
La Rambla
Tapa Viento
Rio Cuarto
Volcán Platanar
2183 m.
R.V.S. Bosque Alegre
San Miguel
Horquetas
Col. del Toro
ngeles
P.N. Juan Castro Blanco
Cariblanco
San Jorge
Sardinal
Rita
Roxana
Montaña
P.N. Volcán Poás
2708 m.
P.N. Braulio Carrillo
Palmira
Corinto
Santa Clara
Flores
PT-2
GUAPILES
Bajos del Tor
ZARCERO
Poasito
Vara Blanca
Volcán Barva
2906 m.
Fraijanes
Cartagos
Sacramento
SARCHI
SAN PEDRO
La Cruz
Birri
San Jos de la Montaña
GRECIA
ALAJUELA
HEREDIA
P.N. Volcán Turrialba
3328 m
P.N. Volcan Iraz
3432 m.
SAN ISIDRO
Rancho Redondo
Santa Cruz
Turrucares
Balsa
SANTA ANA
Llano Grande
San Juan
Chicoá
La Pastora
PACAYAS
SAN PABLO
Z.P. El Rodeo
SAN JOSE
TRES RIOS
Cot
CARTAGO
JUAN

UMASS JPL

AIRSAR Flight Lines

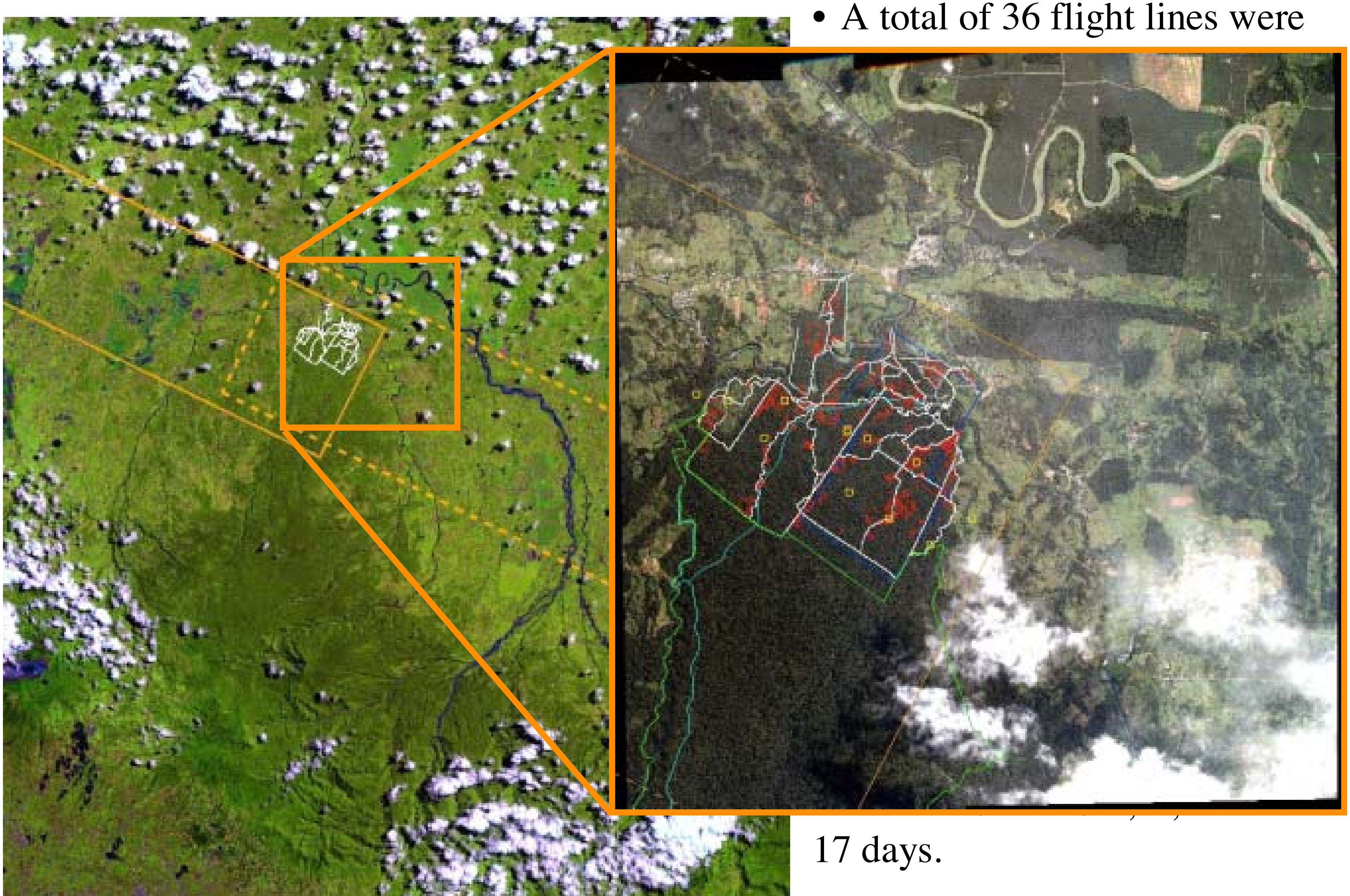

- A total of 36 flight lines were

17 days.

Lidar Coverage (DEM & vegetation height)

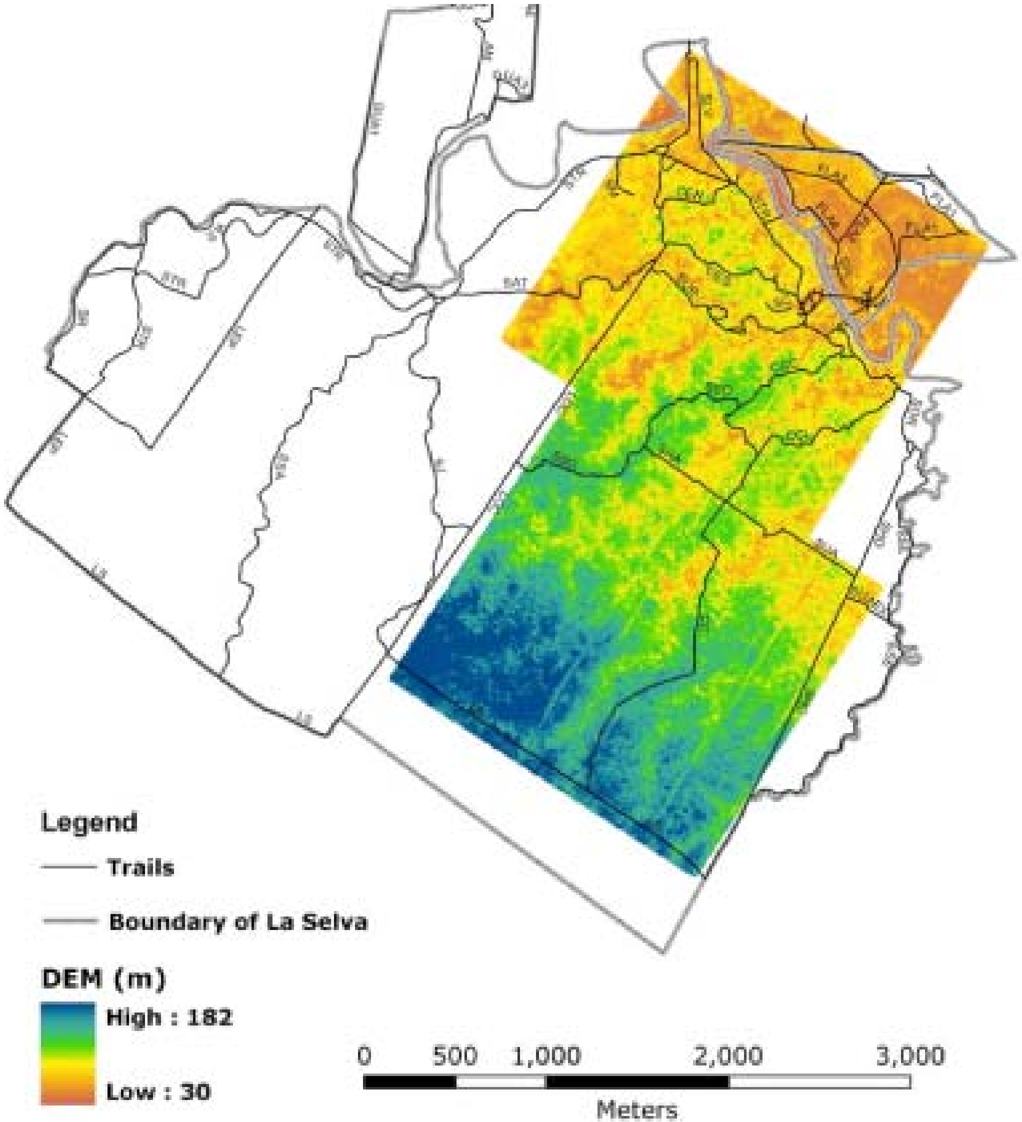

A Visit From the Top

Site Overview

Deployment Logistics

Secondary Regrowth Test Sites

Paul Siqueira Slide # 42

Deploying Corner Reflectors

• The La Selva Biostation is located about 80 km north of the capitol, San Jose.

• Within the reserve are well studied stands ranging in age from 1-2 year regrowth to mature tropical forests.

• LVIS LIDAR ground surface DEM and canopy heights are available for a portion of the reserve.

• Corner reflectors were deployed in open areas within the reserve.

• Reflectors were oriented to be visible on both the 124° and 296° heading flight lines.

Vegetation Photos

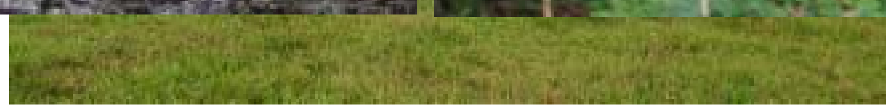

Site Survey or Goofing Off?


Shouldn’t you guys be doing lidar?

Flight Plans

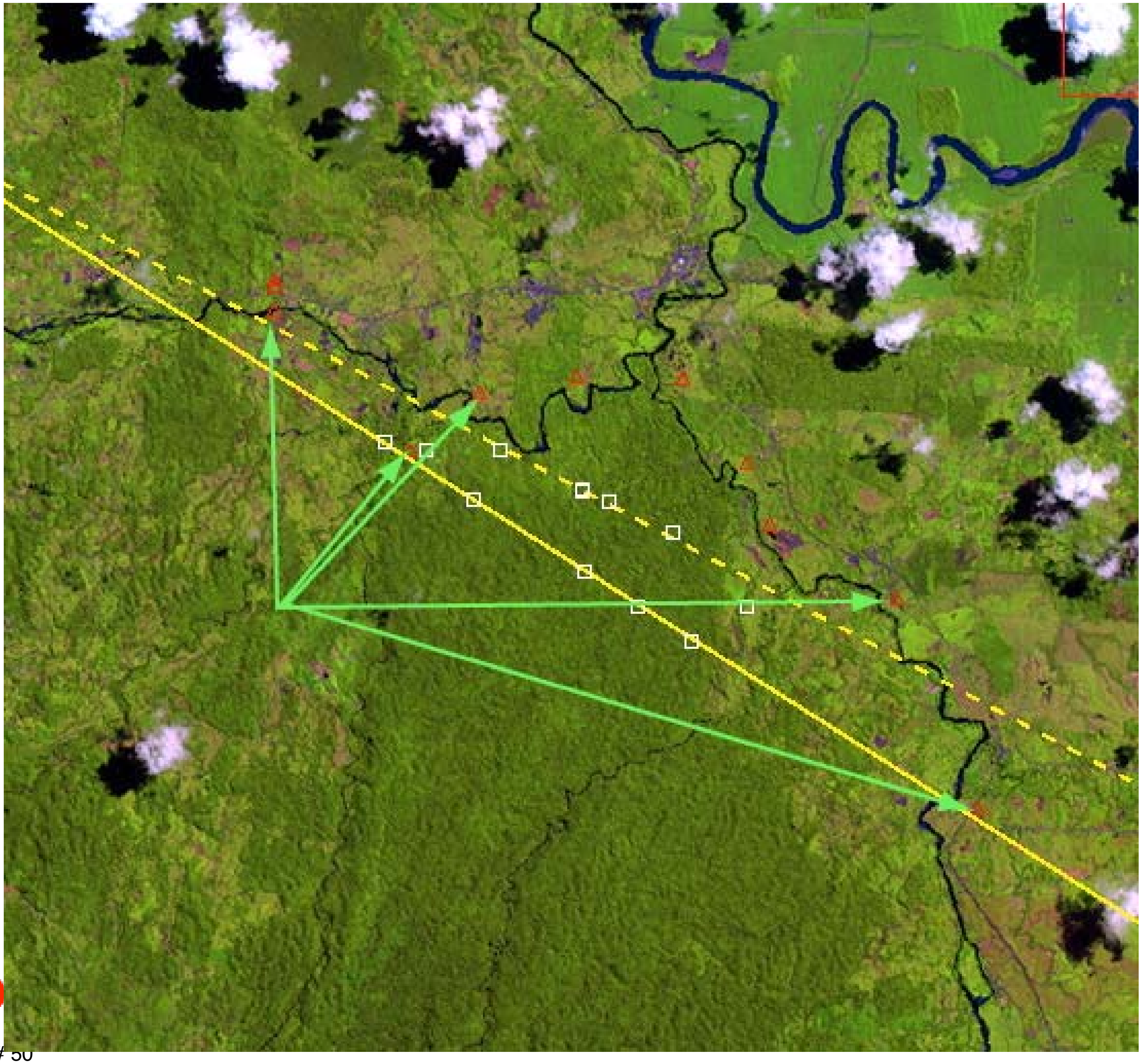

Wave Number Diversity at La Selva

• The vertical wave number, that depends on range, baseline and wavelength, determines the sensitivity of the interferometer to vertical structure or vegetation height.

$$\gamma = \gamma_v \prod_{k=1}^{N} \gamma_k = \frac{\int_{h_b}^{h_t} \sigma(z) e^{ik_z z} dz}{\int_{h_b}^{h_t} \sigma(z) dz} \prod_{k=1}^{N} \gamma_k = e^{-ik_z (h_t - h_b)/2} \operatorname{sinc}\left(\frac{k_z (h_t - h_b)}{2} \right) \prod_{k=1}^{N} \gamma_k$$

$$k_z = \frac{2\pi pb \cos(\theta - \alpha)}{\lambda \rho}$$

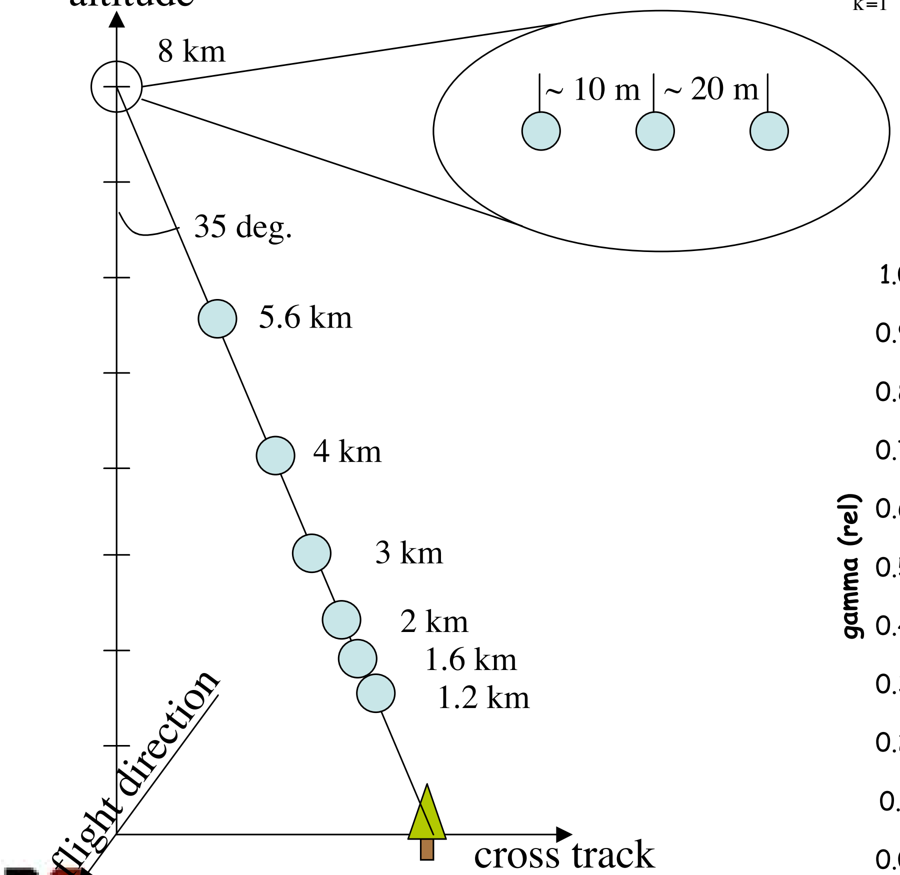

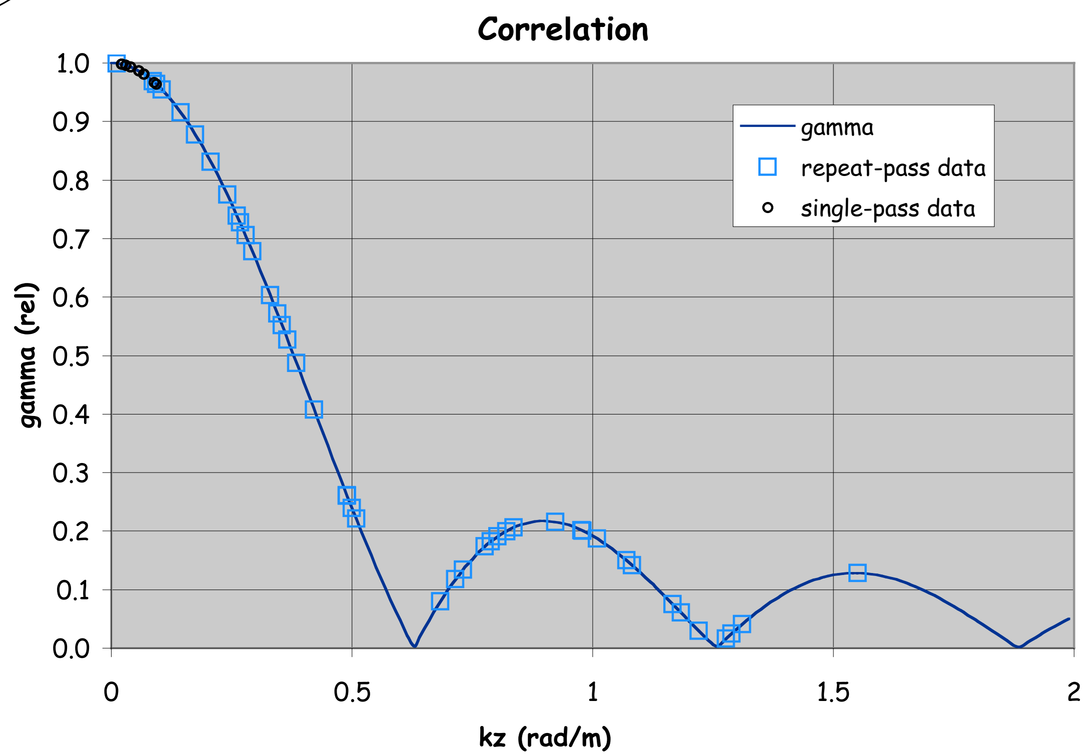

AIRSAR Repeat Pass Flight Line Geometry

- Two aircraft headings were used for repeat-pass interferometry at La Selva (124° & 296°), collected over three days (March 3, 6, and 20 of 2004).

- Shown below are the cross-track and altitude changes for +/- 5km along-track distance to the La Selva OTS facility.

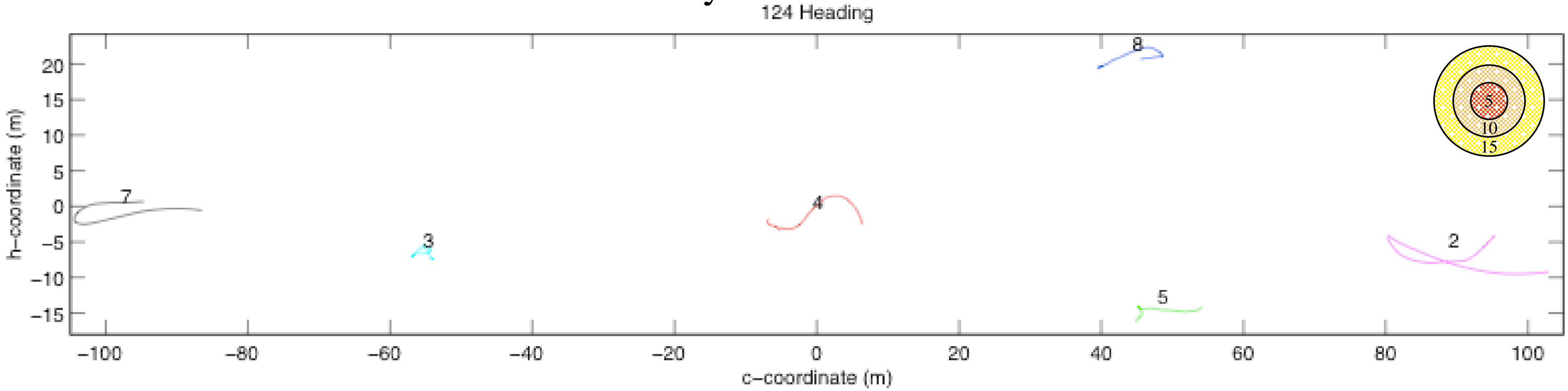

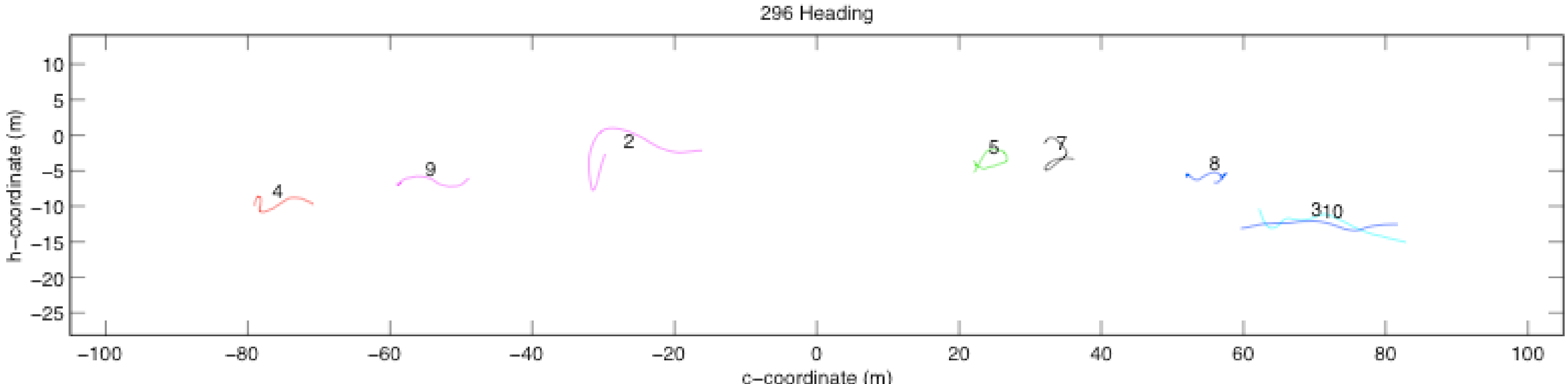

Data Analysis

Interferometric Baselines

- Flight lines may be combined to form various interferometric pairs
- Shown below are the perpendicular baseline (Bp) and perpendicular baseline variations (standard deviation) for various interferometric pairs, as well as the time between pairs (in hours; 72 hrs = 3 days)
- Pairs are sorted in order of descending perpendicular baseline.

hdg	set #1	set #2	Δt (hrs)	B(m)	α(deg)	Bp (m)	stdev(Bp)
296	3	10	-71.53	2.50	63.75	1.1	1.6
296	5	7	-74.17	9.80	-37.54	8.6	2.8
296	3	8	-72.64	15.96	-28.24	9.2	6.2
296	8	10	1.11	17.61	151.05	10.3	7.0
124	5	8	-73.67	36.22	-84.32	14.7	6.1
296	7	8	0.50	21.72	171.79	17.1	2.9
296	4	9	-72.66	21.85	-171.45	20.2	4.9
124	2	8	-72.13	52.41	-32.09	24.7	5.7
296	5	8	-73.67	31.06	175.85	25.7	1.5
296	2	9	-71.64	27.98	7.18	25.8	7.7
296	3	7	-73.14	36.98	-14.61	26.3	4.2
296	7	10	1.61	38.57	165.11	27.4	5.2
124	3	7	-73.14	42.99	-8.08	33.9	4.0
296	3	5	1.03	46.15	-11.01	34.9	5.4
124	4	5	0.52	50.55	164.09	35.4	7.2
296	5	10	-72.56	47.71	168.75	36.0	6.0
124	2	5	1.54	41.75	11.27	39.4	5.7
296	2	5	1.54	51.67	69.54	44.3	5.3
296	2	4	1.02	49.82	7.77	46.0	3.2
124	3	4	0.51	54.94	-174.46	50.0	4.6
124	4	8	-73.15	50.21	-153.93	50.1	1.8
296	2	7	-72.63	61.28	38.9	52.9	5.8
296	2	8	-72.13	82.69	107.46	70.0	3.9

hdg	set #1	set #2	Δt (hrs)	B(m)	α(deg)	Bp (m)	stdev(Bp)
296	5	9	-73.18	79.34	2.12	70.1	3.9
124	2	4	1.02	89.76	-3.49	74.8	5.6
296	7	9	0.99	88.90	2.36	78.7	2.6
296	2	3	0.51	97.42	174.32	79.2	9.2
296	2	10	-71.02	98.96	174.13	80.3	10.4
124	4	7	-73.65	97.22	-0.4	83.9	7.7
124	3	5	1.03	103.60	175.55	85.4	2.7
296	4	5	0.52	101.06	-176.59	90.4	3.3
296	8	9	0.49	110.26	0.36	95.8	4.6
296	4	7	-73.65	110.61	-176.54	99.0	2.7
124	3	8	-72.64	103.45	-164.63	100.1	3.7
296	3	9	-72.15	124.71	-2.63	105.0	1.7
296	9	10	0.62	126.24	177.2	106.1	2.7
296	4	8	-73.15	131.90	-178.37	116.1	2.1
124	5	7	-74.17	146.52	-5.5	119.3	3.6
124	2	3	0.51	144.22	-0.03	124.8	4.4
296	3	4	0.51	146.19	-1.04	125.3	6.4
296	4	10	-72.04	147.71	178.8	126.4	7.5
124	7	8	0.50	143.92	-171.42	134.0	7.3
124	2	7	-72.63	186.87	-1.86	158.7	3.7

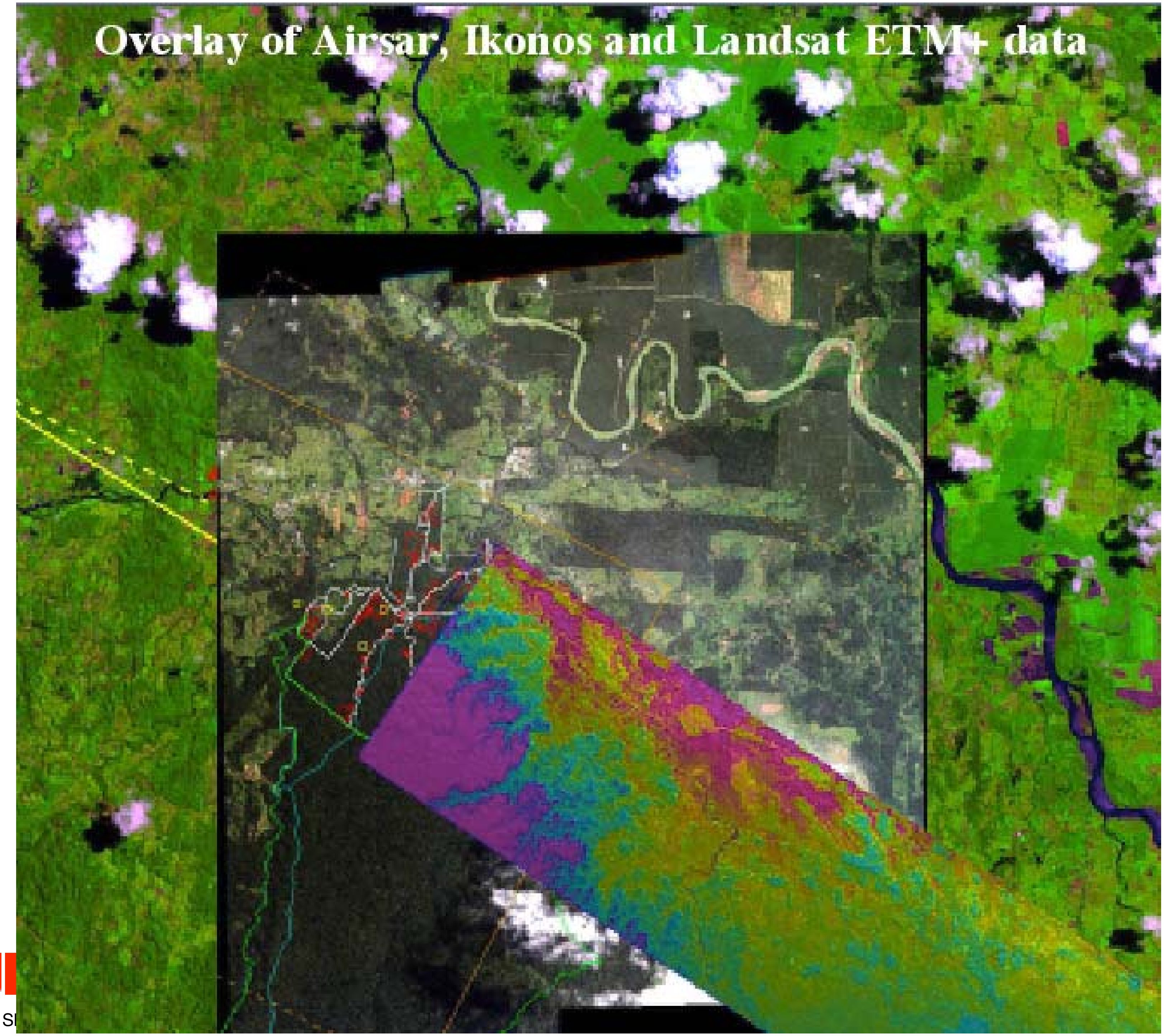
Overlay of Airsar, Ikonos and Landsat ETM+ data

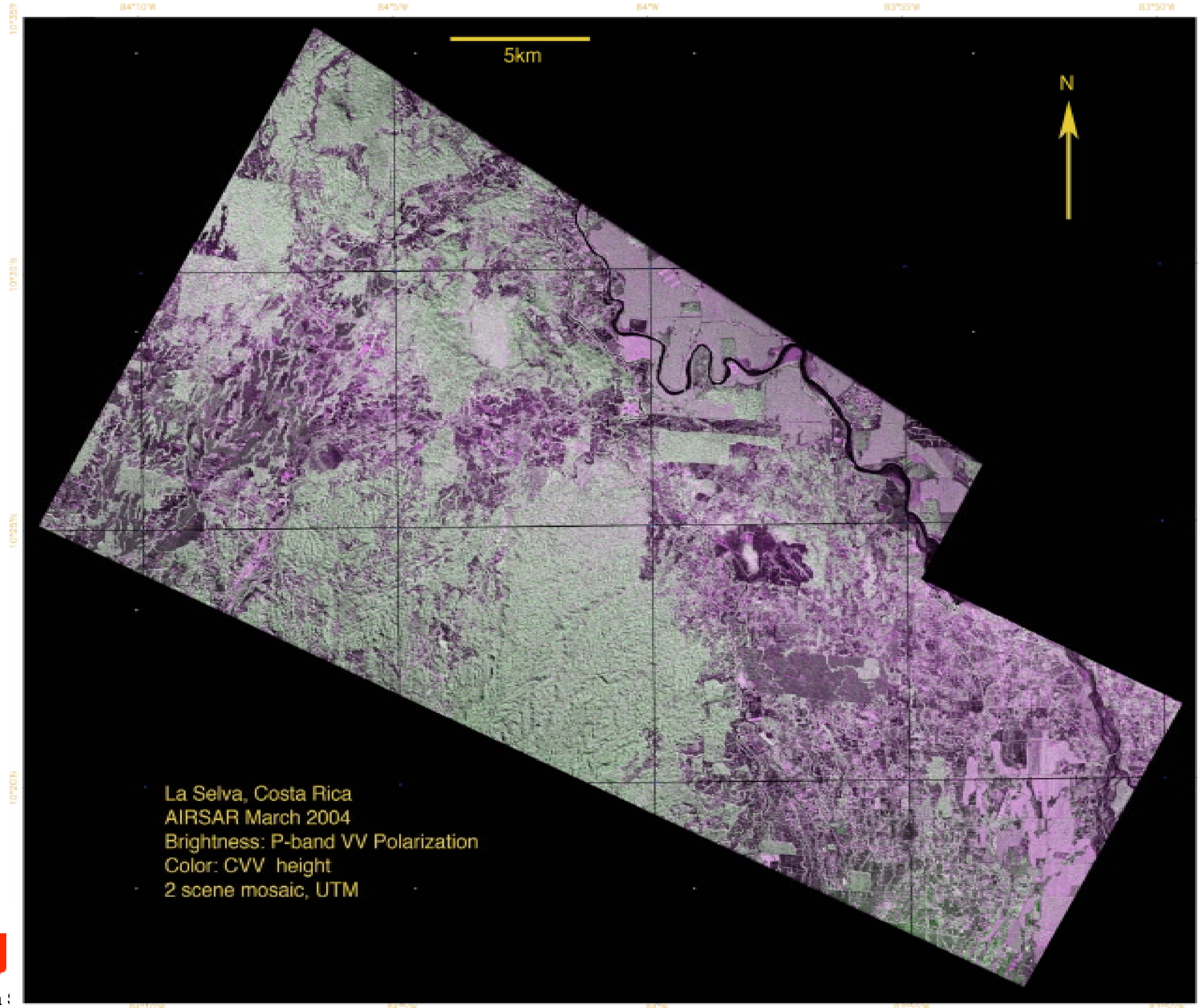

UMASS

Paul Siqueira

La Selva Site

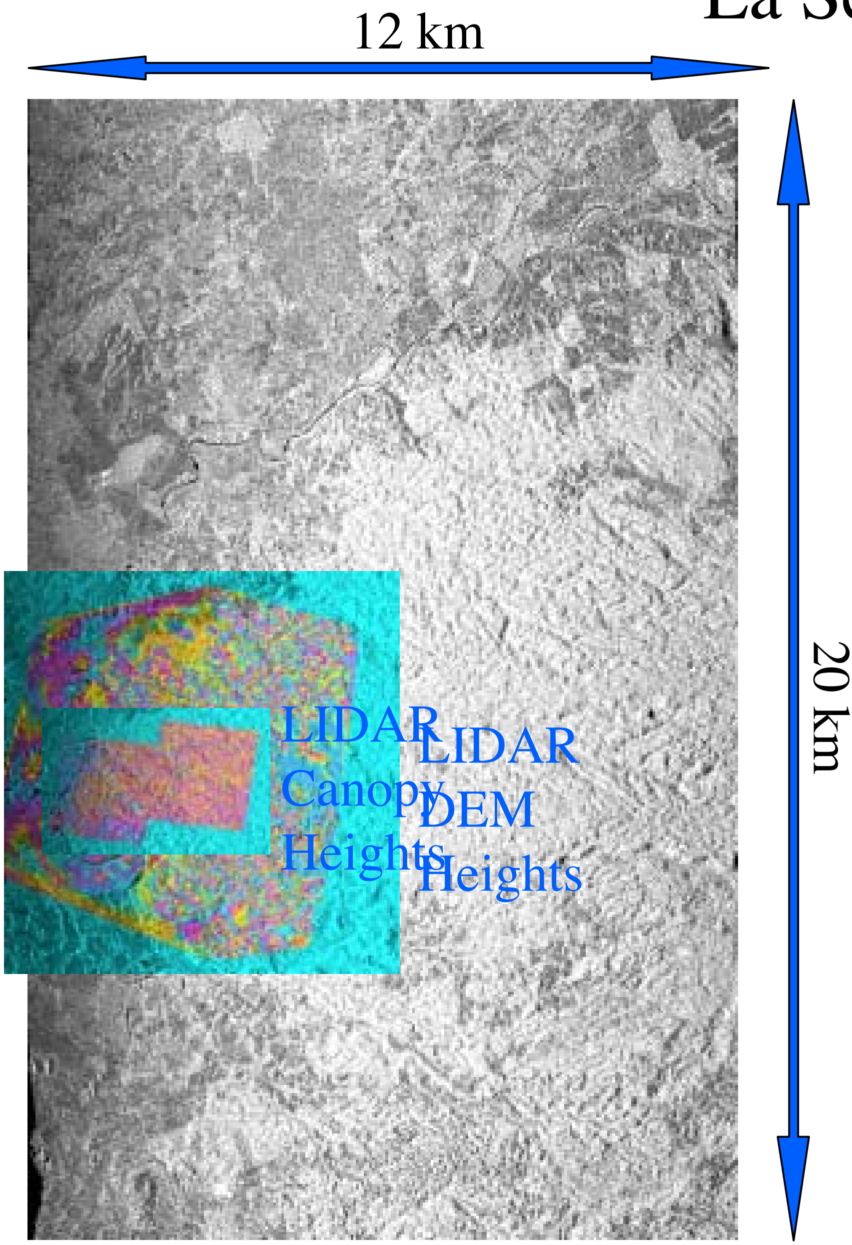

L-band VV Imagery

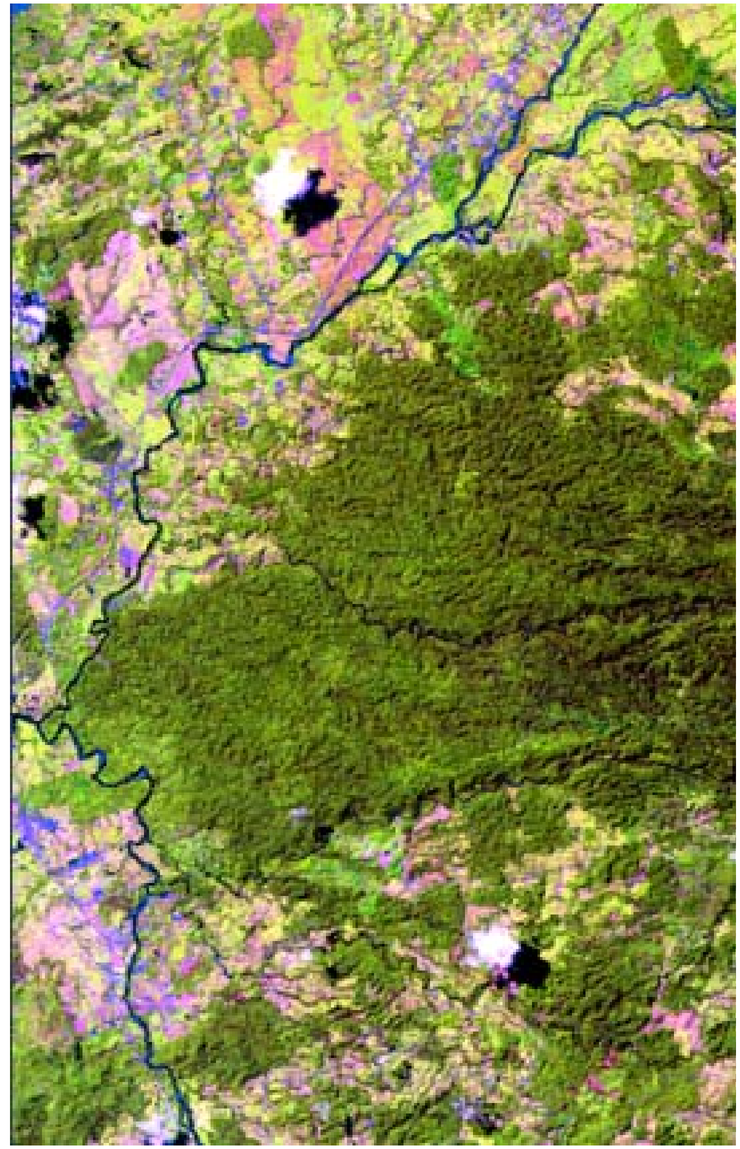

Landsat Imagery

L-band RPI 20-30 m Baseline

Magnitude

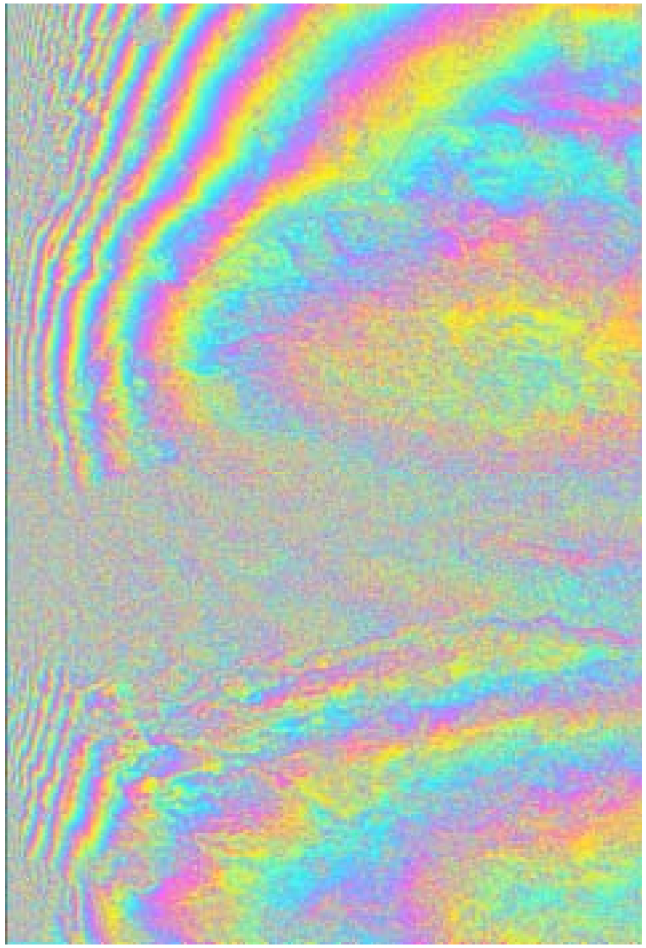

Phase

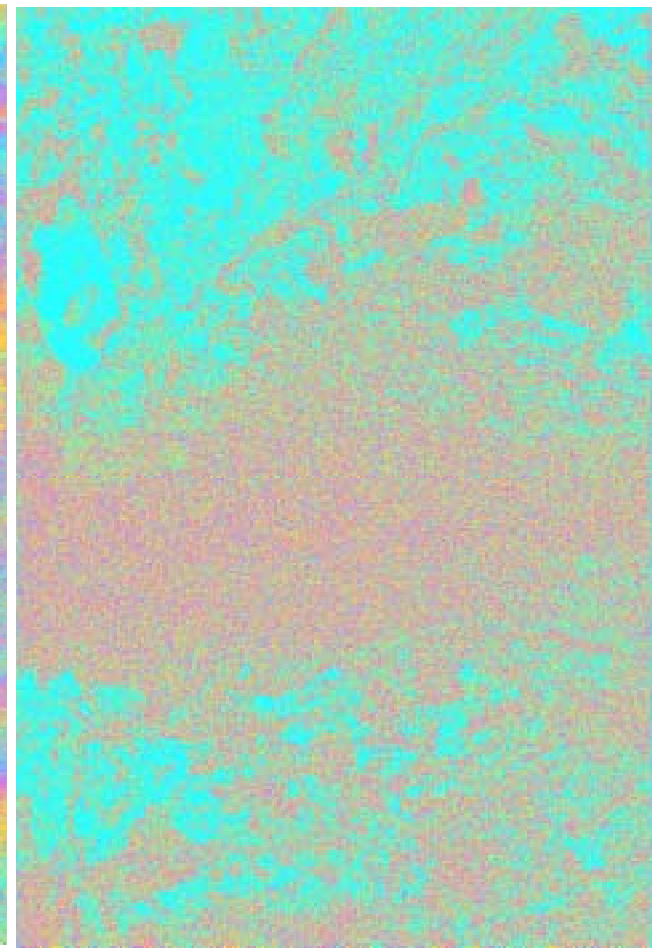

Correlation

• L-band repeat pass data collected on March 3, 2004 from passes 296-1 and 296-2. Interferometric baseline varies between 20 m and 35 m depending on location along-track.

Correlation Comparison

L-band SPI DEM (2.2 m)

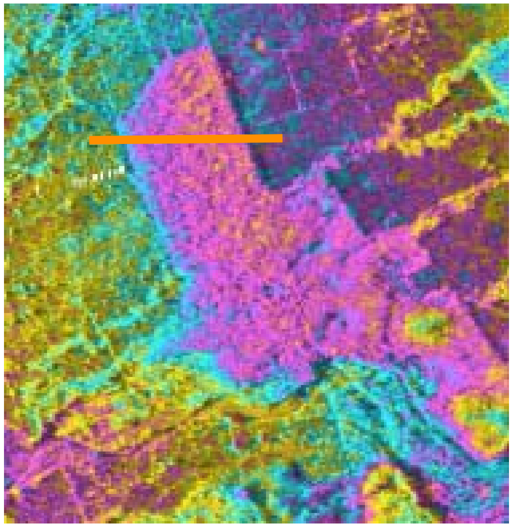

L-band SPI Correlation

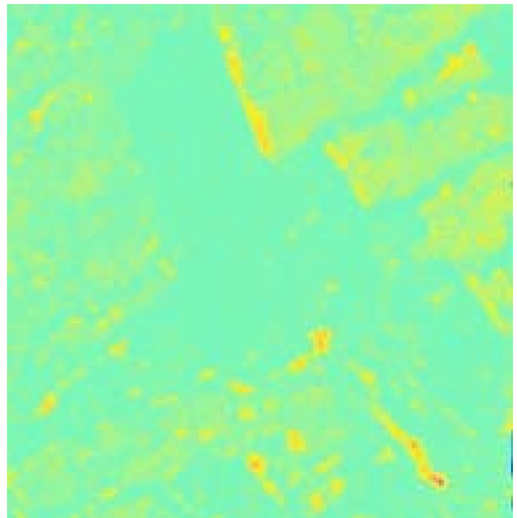

L-band 20 m Correlation

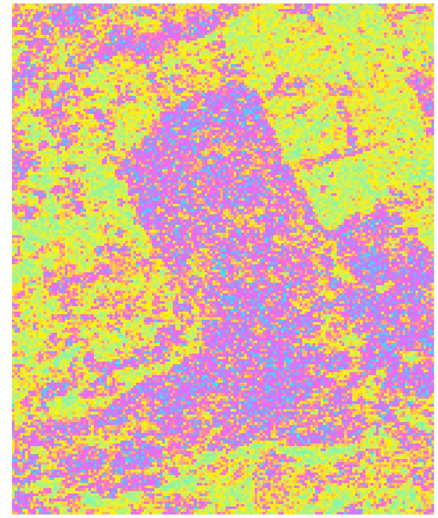

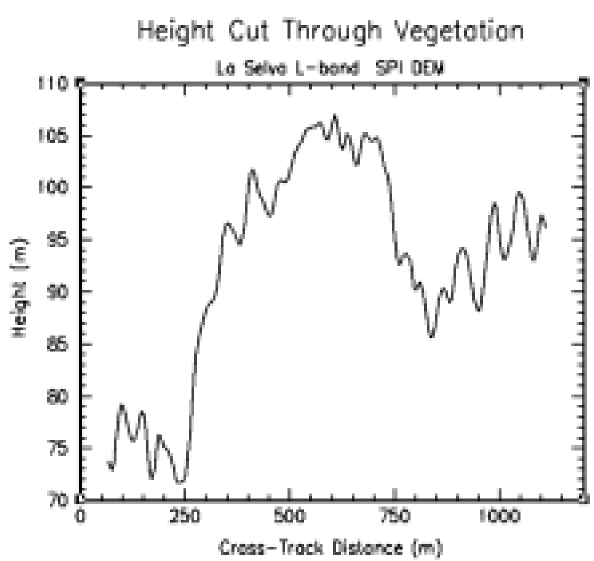

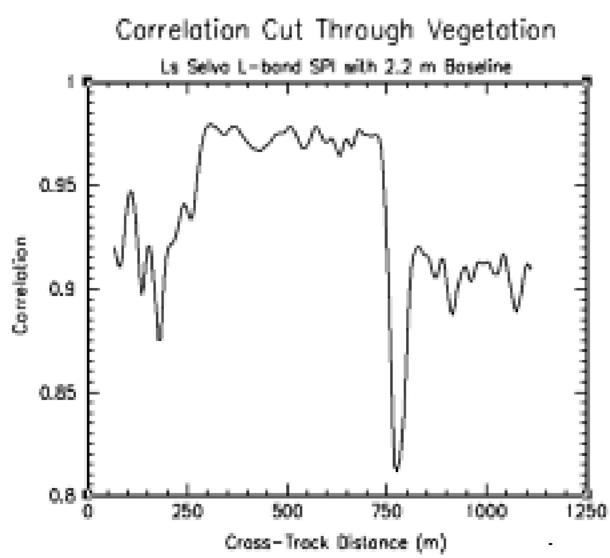

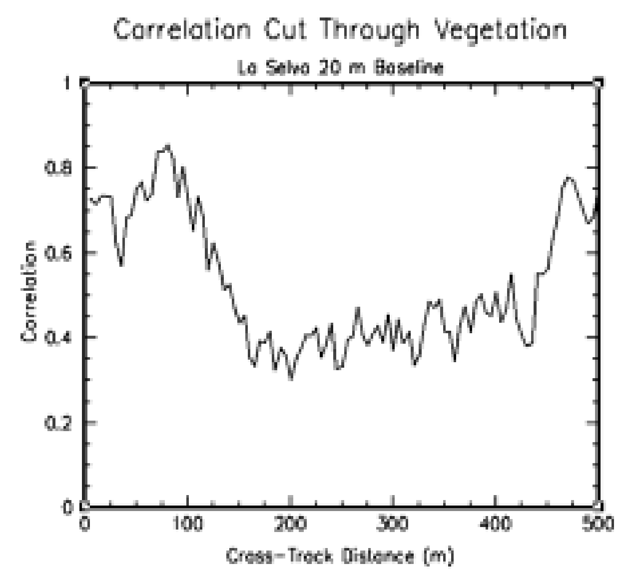

L-band 20 m Baseline Tree Height Estimates from Correlation

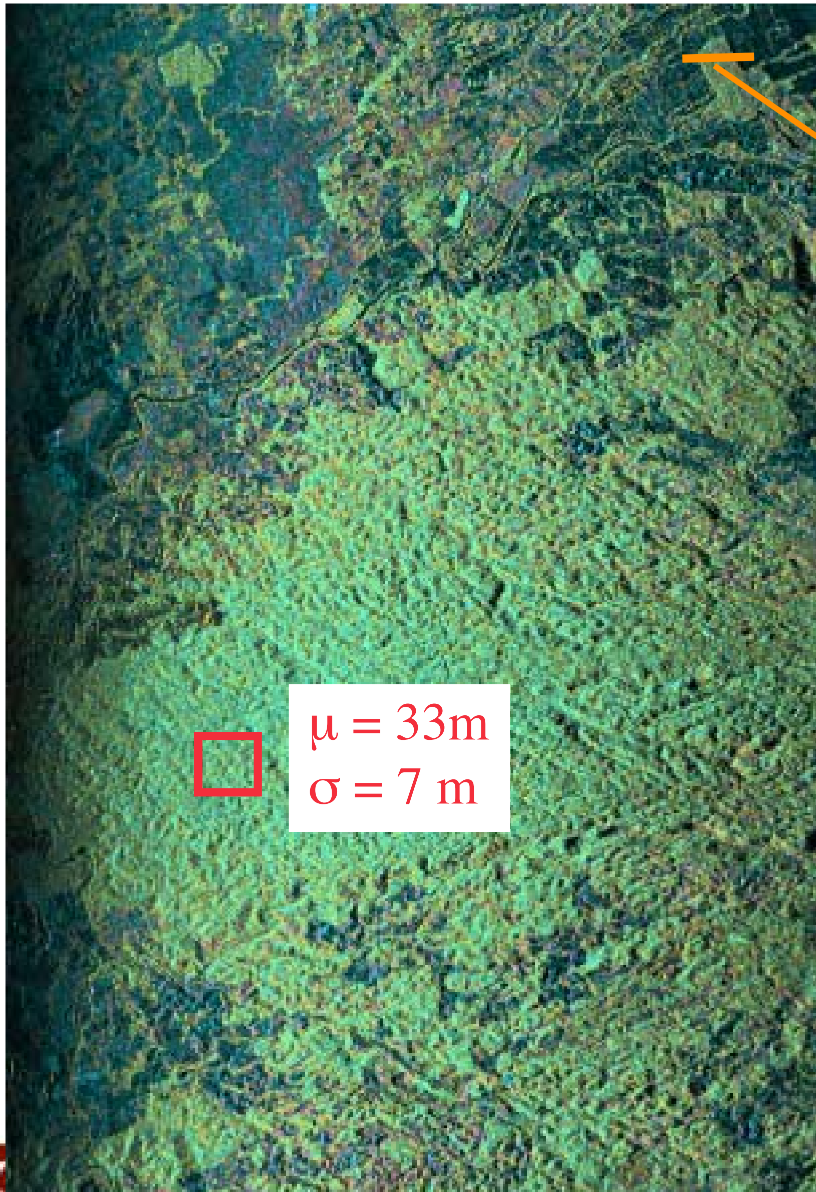

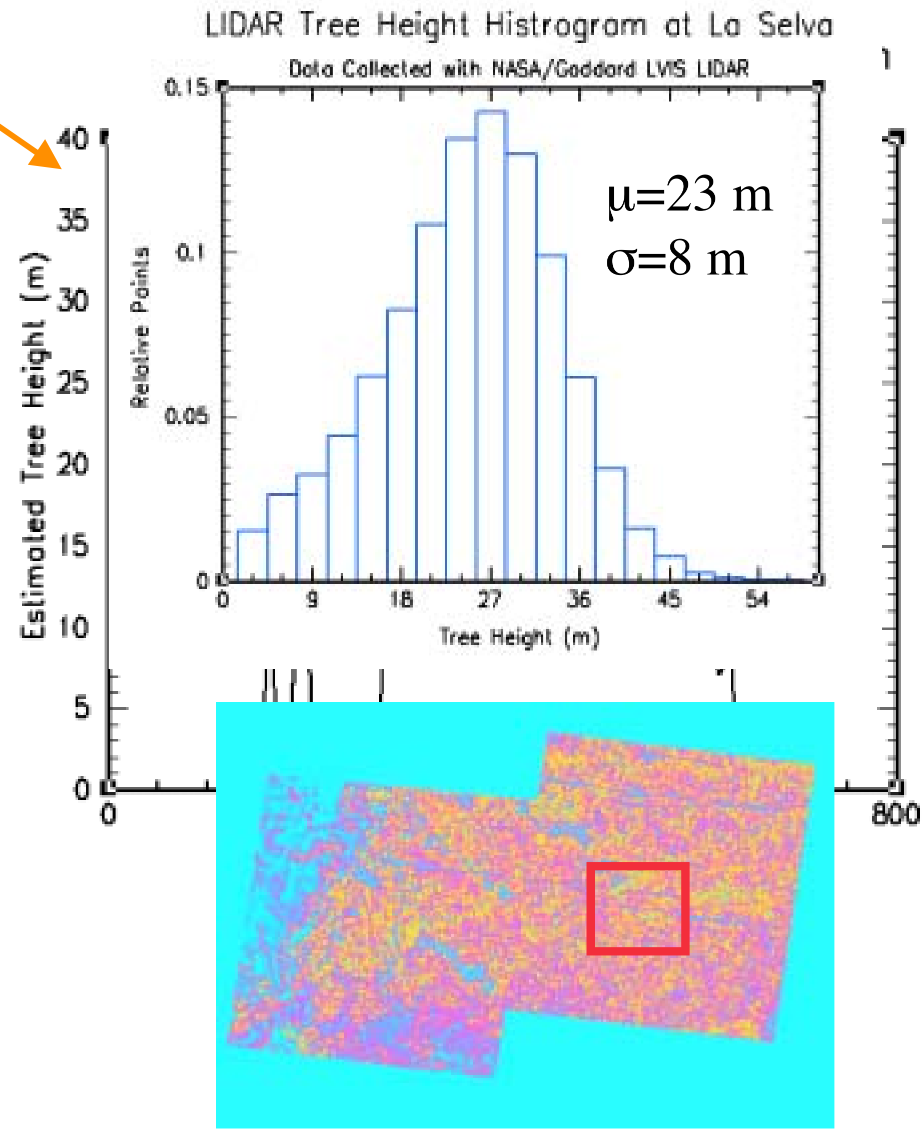

L-band Polarimetric Correlations - 100 m Baseline

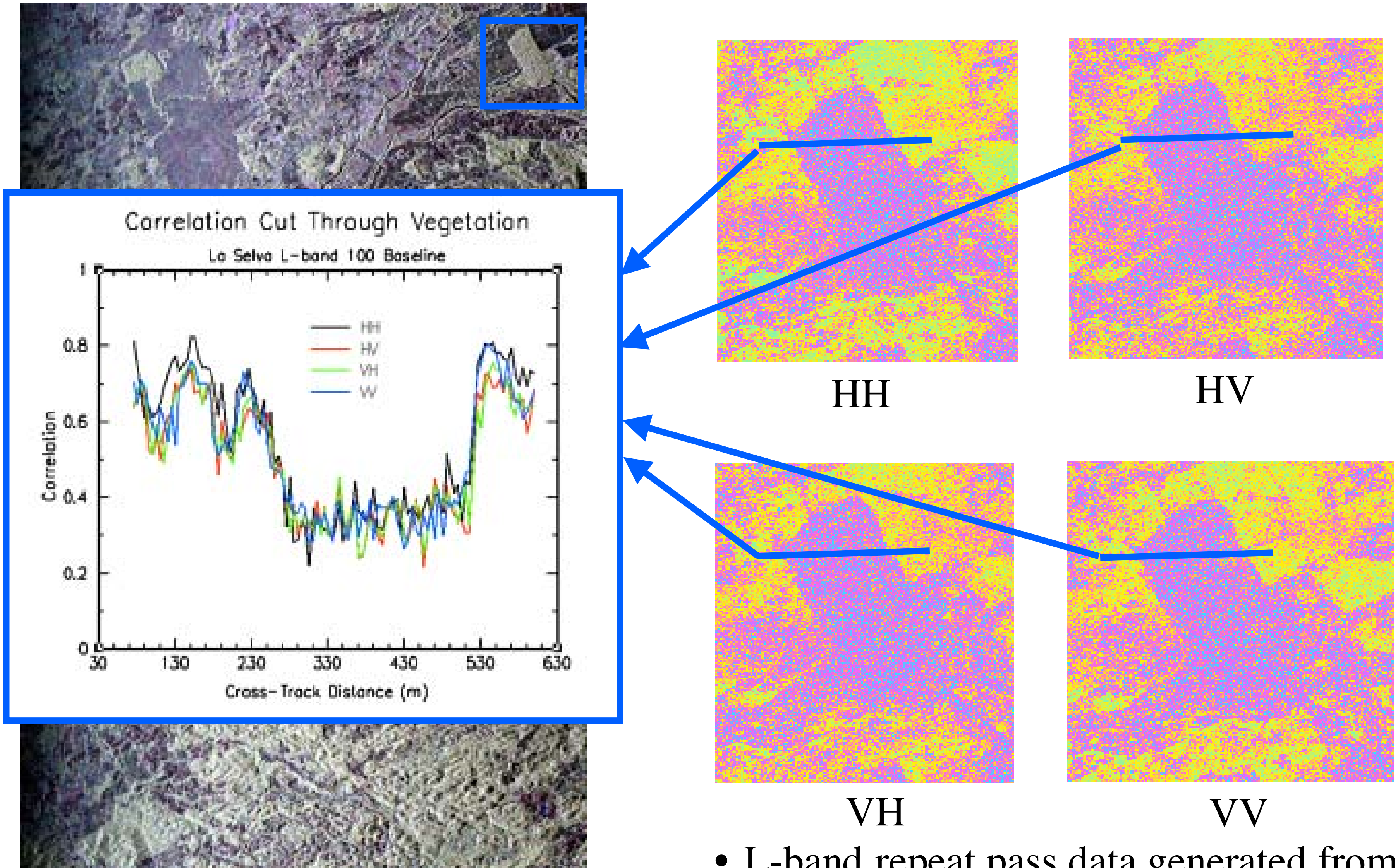

L-band Polarimetric Imagery from 296-10

- L-band repeat pass data generated from flight lines 296-10 and 296-11 having a 100 m baseline.

P-band 20 m Baseline Interferogram

P-band Polarimetric Imagery

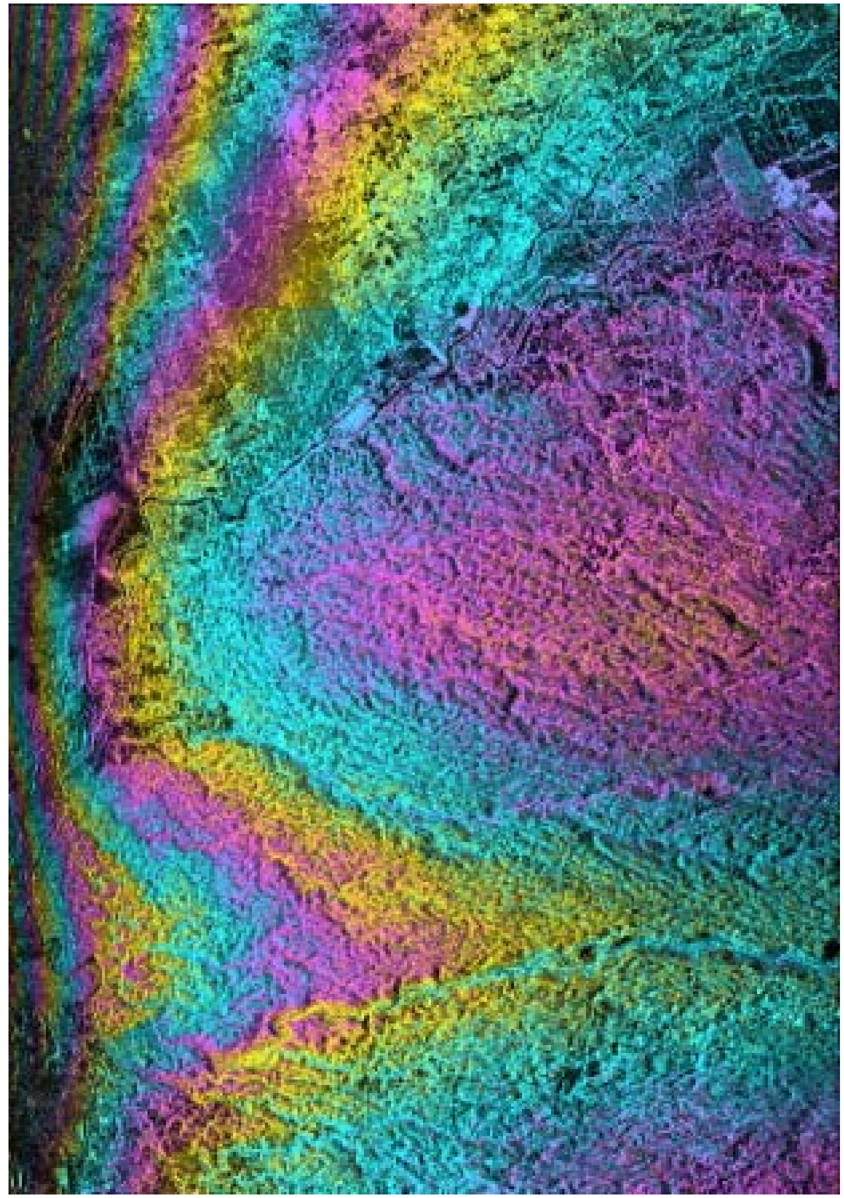

Flight Lines 296-1 and 296-2

P-band Polarimetric 20 m Baseline Interferometry

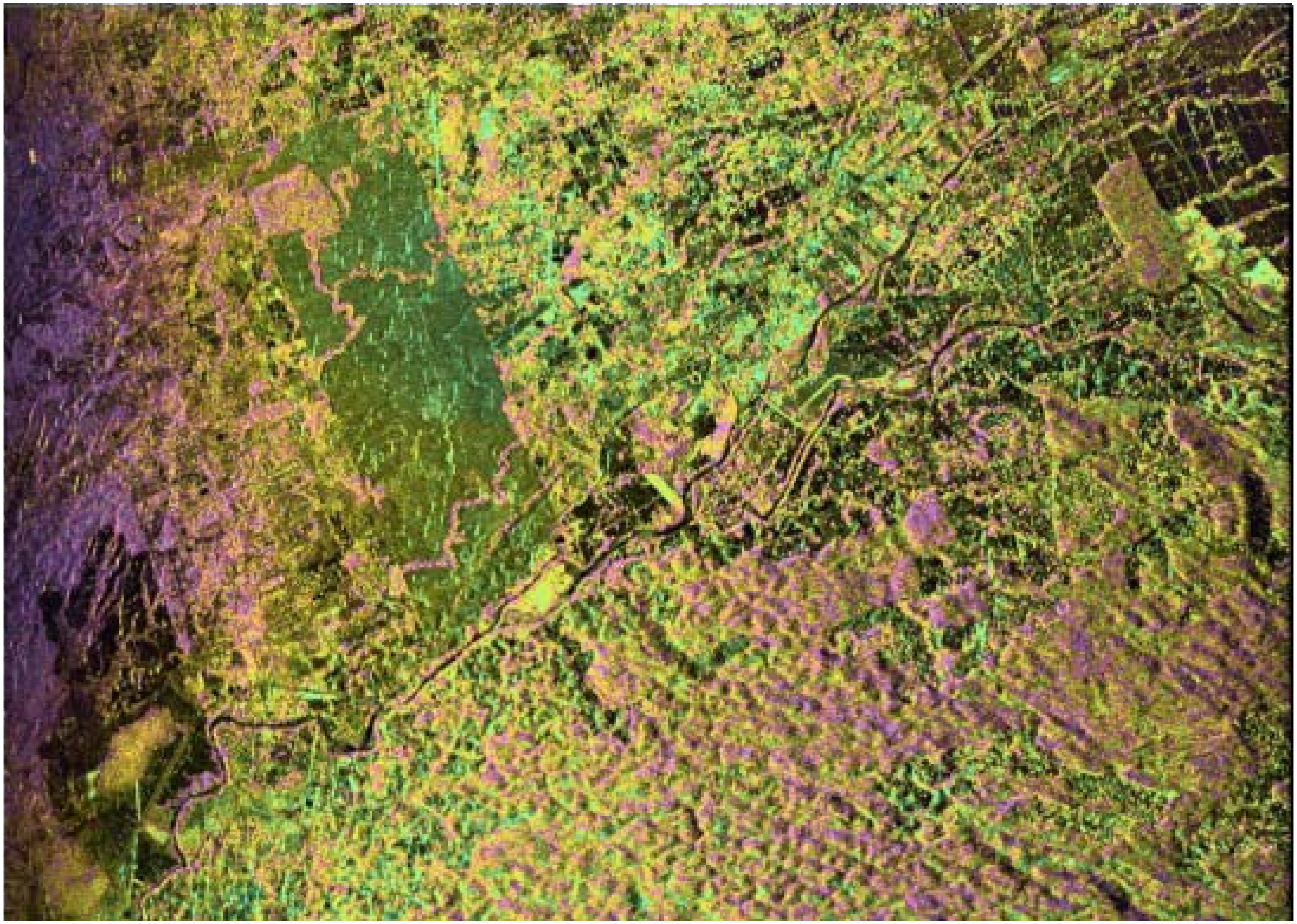

PHH image from the 296-1 and 296-2 20 m baseline interferometric pair.

P-band Polarimetric Correlation Maps

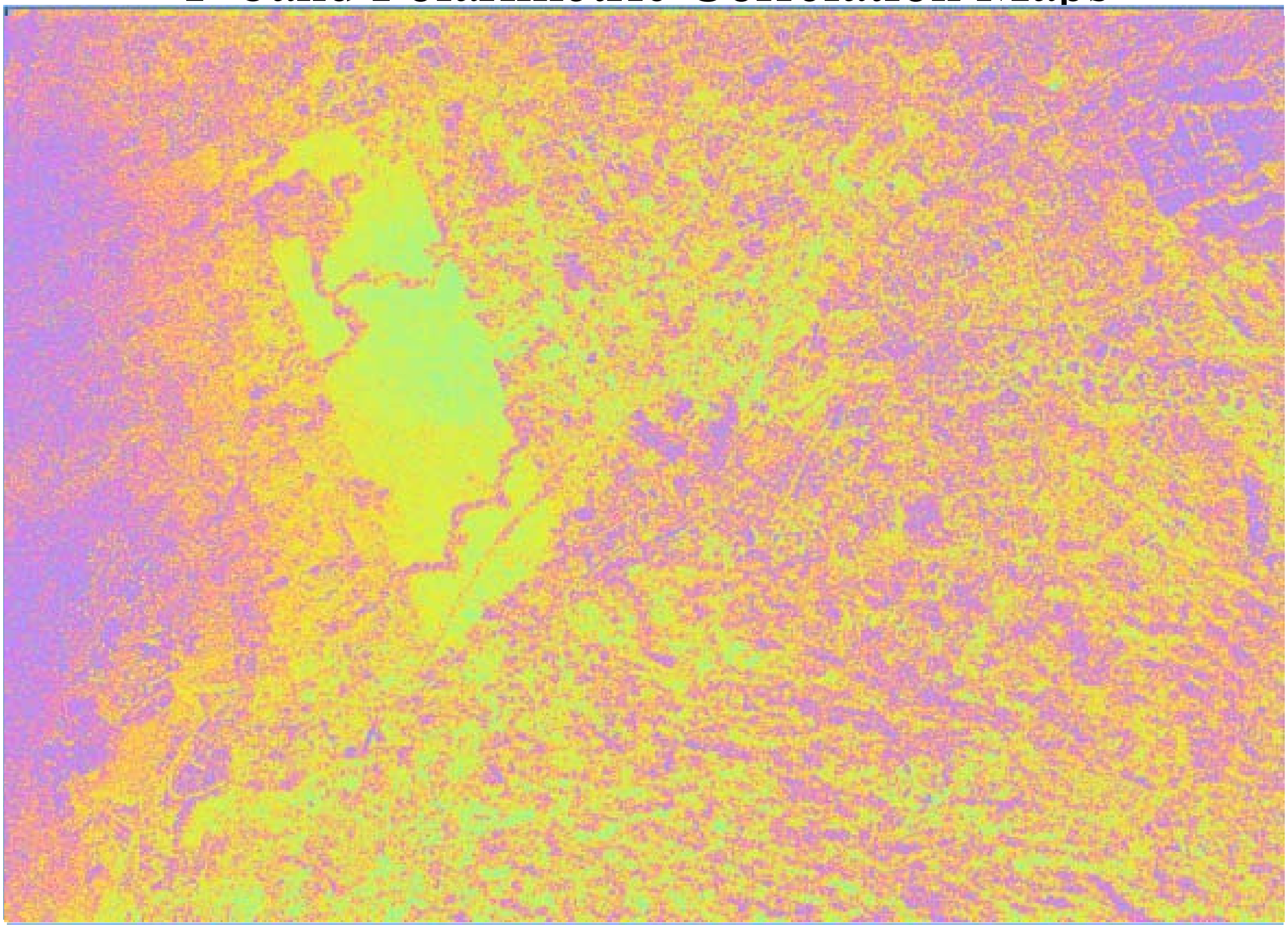

PNVH

Conclusions and Future Work

Conclusions

- Over one year has passed since the last meeting this work was presented in this venue

- Since then, we have
    - addressed the issue of chosing a baseline (more to be done both pre- and post-launch)
    - effect on deformation observing strategy has been quantified and demonstrated to not be an issue
    - orbital issues have been investigated and found not to be a significant problem
    - temporal decorrelation studies have been performed and are actively under way.

- In the near term we want to be active members in PALSAR calibration
    - Raw, level zero, reformatted signal data is requested
    - A variety of repeat-pass baselines over short time periods
    - Both quad-pol and dual-pol data…

Dual Pol vs. Quad Pol

- keep in mind that quad-pol requires 2x PRF, and so there are tradeoffs to be considered in chosing the best observing strategy.

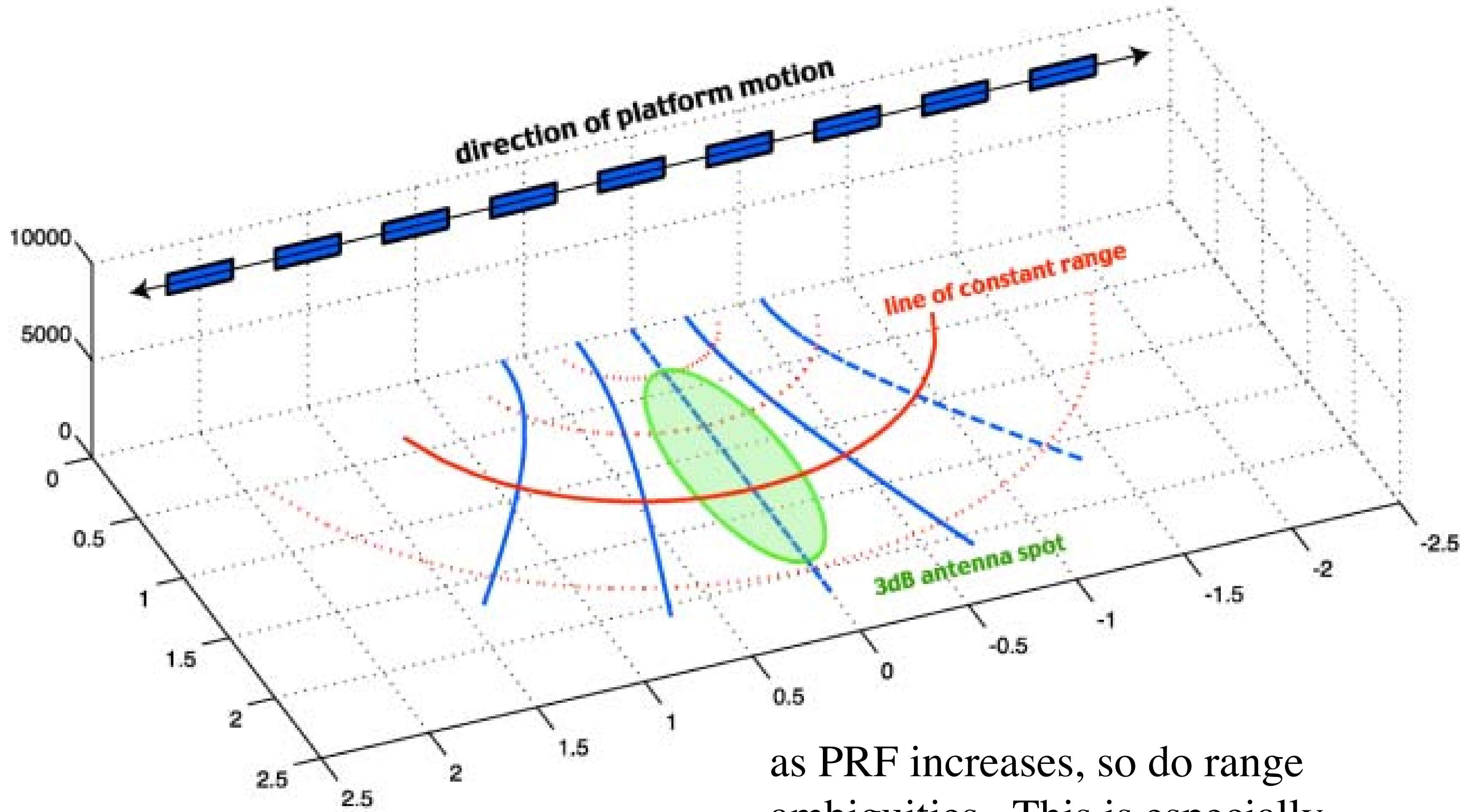

as PRF increases, so do range ambiguities. This is especially problematic for cross-pol measurements

What Next?

MIRSL's mission is to train students for careers in engineering and the physical sciences through research and development of innovative instrumentation and techniques for remote sensing of the environment.

close collaboration with JPL to continue.

End